

Distribution Agreement

In presenting this dissertation as a partial fulfillment of the requirements for an advanced degree from Emory University, I agree that the Library of the University shall make it available for inspection and circulation in accordance with its regulations governing materials of this type. I agree that permission to copy from, or to publish, this dissertation may be granted by the professor under whose direction it was written, or in his absence, by the Dean of the Graduate School when such copying or publication is solely for scholarly purposes and does not involve financial gain. It is understood, that any copying from, or publication of, this dissertation which involves potential financial gain will not be allowed without written permission.

Signature

Suleyman Ucuncuoglu

Date

Single Molecule Characterization of RNA Polymerase I: Technique, Instrumentation & Experimental Development

By
Suleyman Ucuncuoglu

Doctor of Philosophy
Physics

Advisor: Dr. Laura Finzi

Approved for the Department by:

Advisor

Dr. David Dunlap
Committee Member

Dr. Connie Roth
Committee Member

Dr. Kurt Warncke
Committee Member

Dr. Eric Weeks
Committee Member

Accepted:

Lisa A. Tedesco, Ph.D. Dean of the Graduate School

Date

Single Molecule Characterization of RNA Polymerase I: Technique, Instrumentation & Experimental Development

By

Suleyman Ucuncuoglu

B.S., Bogazici University

Turkey, 2005

Advisor

Laura Finzi, Ph. D.

An Abstract of
A Dissertation submitted to the Faculty of the
James T. Laney Graduate School Studies of Emory University
in partial fulfillment of the requirements for the degree of
Doctor of Philosophy
in Physics

2014

Abstract

Single Molecule Characterization of RNA Polymerase I: Technique, Instrumentation & Experimental Development

By Suleyman Ucuncuoglu

Transcription is the prerequisite of protein synthesis. Indeed, as the factory for proteins, the ribosome is predominantly built by rRNA. In eukaryotes, this particular RNA is transcribed from rDNA genes by RNA Polymerase I (Pol I). Therefore, transcription of rDNA is vital for cellular growth and biogenesis. Pol I should produce sufficient amounts of rRNA to fulfill the increasing demand for ribosomes in the cell. The activity of Pol I is regulated up to four fold during the cell cycle, but in all, Pol I accomplishes more than 60% of the all transcription in the cell. Although Pol I is responsible for the majority of the transcriptional activity in the cell, the information related to its kinetics and mechanism is limited. This dissertation focuses on the development and use of an experimental strategy to characterize the dynamic properties of Pol I elongation. In particular, the first single molecule assay was established for monitoring Pol I elongation, and multiplexing tethered particle motion (TPM) measurements were succeeded in to simultaneously monitor hundreds of single molecules. This technical improvement was dictated by the low yield of elongating Pol I complexes. When compared to the conventional TPM setup, the throughput of the experiments was increased up to 10 fold. This new TPM setup, Pol I elongation rate, and possible pause locations along the rDNA template were measured. The average elongation rate measured was 20 nt/s at 200 μ M NTP and the pause free rate was around 50 nt/s which is comparable with the estimated *in vivo* rate. Furthermore, a frequent pause location was identified around 200 bp downstream of the promoter. This finding is in line with the recent finding of a prominent pause location in prokaryotic cells.

In conclusion, the TPM optical and data collection/storage setup was optimized. This system was used to directly measure the elongation rate of Pol I and its pause probability along the template. These dynamic characteristics provide important insight into the mechanism of Pol I transcriptional elongation which may be valuable in engineering anticancer drugs aimed at stopping cell proliferation by interfering with ribosome assembly.

Single Molecule Characterization of RNA Polymerase I: Technique, Instrumentation & Experimental Development

By

Suleyman Ucuncuoglu

B.S., Bogazici University

Turkey, 2005

Advisor

Laura Finzi, Ph.D.

A Dissertation submitted to the Faculty of the
James T. Laney Graduate School Studies of Emory University
in partial fulfillment of the requirements for the degree of
Doctor of Philosophy
in Physics

Acknowledgements

Foremost, I would like to express my sincere appreciation to my advisor Dr. Laura Finzi for her guidance, support and many fruitful discussions during these last four years. I learned a lot from her especially how important to be organized in science. I would like to thank her for encouraging me to be an independent researcher. I also owe my deepest gratitude to Dr. David Dunlap for the stimulating discussions and great ideas. I have learned so much more than making gel assays and growing cell cultures in his lab.

I also would like to thank my committee members Dr. David Dunlap, Dr. Connie Roth, Dr. Kurt Warncke and Dr. Eric Weeks for following my progress, giving advices and steering me in the right directions. I would like to thank Dr. Weeks for suggesting the random walk analysis and the particle tracking discussions. I would like to thank Dr. Warncke for guiding me for the kinetic analysis. I would like to thank Dr. Roth for the discussions for the polymer nature of the DNA. I also would like to thank my committee members for critical reading of my dissertation.

I must acknowledge the Finzi lab members; Dr. Sandip Kumar, Yan Yan, Dr. Yue Ding, Dr. Monica Fernandez and Dr. Diane Weiner for their help in the laboratory and discussions during the group meetings. I also would like to thank my friends Mustafa Cenap Aydin, Dr. Cem Cakir, Dr. Orhan Ozgur Aybar and Bilal Ayan for their friendship since my college years and reminding me the enthusiasm that I have when I first started studying physics.

I would like to thank my parents, Ruveyda and Cevat Ucuncuoglu, and my sister, Asiye Ozyilmaz, for their continuous support during all levels of my education, especially for their patience during my graduate education when I am away from my country. I also would like to thank my father in law, Selim Parlar, and mother in law, Meryem Parlar, for all the sacrifices that they have made on my behalf, and all the other members of my loving and caring family.

Without love and support of my wife, Neslihan, I would have never been able to complete this dissertation. We started this journey together and I am thankful to her for all the late nights and early mornings, for being my proofreader, editor and critical discussion partner and for understanding me more than anyone. I would like to thank my son, Mehmet Duha (hem bal, hem kaymak), for giving me the greatest happiness, inspiration and reminding me the pleasure of learning.

This dissertation is dedicated to my parents, Nefise Ruveyda and Cevat.

TABLE OF CONTENTS

	Page
Chapter 1	1
Introduction	1
1.1 The Tethered Particle Motion technique (Tethered Particle Microscopy)	2
1.1.1 TPM Experimental Setup	3
1.1.2 Experimental protocol for TPM experiments	4
1.1.3 TPM Measurements	5
1.2 RNA Polymerase	7
1.2.1 Types of RNA Polymerases	8
1.2.2 Transcription by RNA Polymerase I	9
1.2.3 Structure of RNA Polymerase I	10
1.3 Motivation and Hypothesis	11
Chapter 2	14
Calibration of Tethered Particle Motion	14
2.1 Introduction	15
2.2 Materials and Method	16
2.2.1 DNA Preparation	16
2.2.2 Chamber Preparation	18
2.2.3 Particle tracking, Data acquisition, and Instrumentation	19
2.2.4 Data Preprocessing and Drift Calculations	21
2.2.5 Symmetry Test	21
2.3 Results	23
2.3.1 Mean Square Excursion	24
2.4 Conclusion	27

Chapter 3	28
Multiplexed Tethered Particle Motion	29
3.1 Introduction	29
3.2 Materials and Methods	30
3.2.1 Sample Preparation for Transcription experiments	30
3.2.2 Sample Preparation for Gyrase wrapping experiments	32
3.2.3 Chamber assembly	32
3.2.4 Optical Setup	34
3.2.5 Hardware and Software	35
3.2.6 Drift correction and bead selection	37
3.3 Results and Discussion	39
3.3.1 Accuracy of radial symmetry tracking	39
3.3.2 Effect of Averaging Time	42
3.3.3 Comparison of DIC and Dark Field Microscopy	44
3.3.4 Gyrase Wrapping Experiments	47
3.3.5 Effects of Compression on the Movie file	48
3.4 Discussion	51
Chapter 4	52
Single Molecule Measurements of RNA Polymerase I Elongation	52
4.1 Background	53
4.2 Materials and Methods	55
4.2.1 Fabrication of TPM microchambers	55
4.2.2 Preparation of Transcription reagents	56
4.2.3 Sample Preparation	61
4.2.4 TPM Measurements of stalled and elongating Pol I complexes	62
4.2.5 Simulations	62
4.3 Results and Discussion	64
4.3.1 Elongation Rate	66
4.3.2 Processivity RNA Polymerase I	69

4.3.3	Pause sites on rDNA	73
4.3.4	Random Walk Hypothesis	76
4.3.5	Energy Barriers of Elongation	78
4.3.6	Kinetic rate of transcription	79
Chapter 5		83
Conclusions		83
5.1	Prerequisite Experiments: Calibration of TPM Data	84
5.2	A Must for Low Yield of Transcriptional events: Multiplexed TPM	85
5.3	Pol I processivity	86
5.4	Pol I elongation rate and pausing	88
References		92

LIST OF FIGURES

Page

Chapter 1

Figure 1-1 Different experimental design for TPM assays.....	5
Figure 1-2 An illustration of the central dogma.....	7
Figure 1-3 The crystal structure of the 14 subunit-Pol I from <i>Saccharomyces cerevisiae</i>	11

Chapter 2

Figure 2-1 A representative optical setup for tethered particle microscopy with DIC optics.	20
Figure 2-2 Symmetry of bead motion	22
Figure 2-3 Selection of beads based on ρ distributions	23
Figure 2-4 Calibration of root-mean-square excursion versus DNA contour length.....	25
Figure 2-5 Calibration of mean-squared excursion versus DNA contour length	26

Chapter 3

Figure 3-1 Assembly of the chamber for TPM experiments	33
Figure 3-2 The assembled chamber on a microscope slide	34
Figure 3-3 Multiplexed TPM setup.....	35
Figure 3-4 Circular excursion pattern of singly tethered beads.	37
Figure 3-5 The angular distributions of bead positions	38
Figure 3-6 A representative DIC image and the intensity gradients.....	40
Figure 3-7 Comparison of the two tracking algorithms; non-linear 2-D Gaussian fitting (red line) and radial symmetry (black line).....	41
Figure 3-8 Mean square excursion length (ρ square in log axis) vs. time plot in log axis	43

Figure 3-9 Images of representative fields of view in dark field microscopy (top) and DIC microscopy (bottom)	45
Figure 3-10 Comparison of DIC (left) and dark field (right) microscopy measurements	47
Figure 3-11 A representative trace showing gyrase-induced DNA wrapping and unwrapping (top)	48
Figure 3-12 The accuracy of the compressed experimental data.....	50
 Chapter 4	
Figure 4-1 Basal requirements for an efficient <i>in vitro</i> Pol I transcription.....	54
Figure 4-2 Diagram of the downstream DNA template.....	57
Figure 4-3 Diagram of the upstream DNA template.....	58
Figure 4-4 Representative gel images of the purified PCR products for the “Downstream” (left panel) and the “Upstream” rDNA (right panel) templates	60
Figure 4-5 Schematic of experimental setups (Top) and representative elongation trace for the “upstream DNA” template (Bottom).....	65
Figure 4-6 Schematic of experimental setup (Top) and representative elongation trace (Bottom) for the “Downstream DNA” template.....	66
Figure 4-7 Pol I elongation rates.....	67
Figure 4-8 Distribution of rates in the presence of 5 μ M NTPs.....	68
Figure 4-9 Frequency distribution of the elongation rates calculated for control experiments before addition of NTPs	69
Figure 4-10 Pol I processivity measured by TPM	70
Figure 4-11 Pol I processivity measured in bulk	72
Figure 4-12 Histogram (bin size is 20 bp) of lengths of DNA tethers observed during transcription by Pol I	74
Figure 4-13 Distribution of pause locations during elongation (raw data).....	75

Figure 4-14 Comparison of the pause locations obtained from experiments (pink) and from biased random walk simulations (blue)..... 77

Figure 4-15 Free energy for the rDNA template (bottom, black) was found by adding base pair stacking energy (top, red) to the hydrogen bonding energy (center, purple) 79

Figure 4-16 The kinetic diagram for the transcription by Pol I which consists of the conversion from open complex to elongation complex with the kinetic rate, k_1 80

Figure 4-17 The simulation for a kinetic model of 4.16 82

LIST OF TABLES

Page

Chapter 2 Calibration of Tethered Particle Motion

Table 2.1 DNA tether lengths for calibration experiments 17

Table 2.2 DNA tethers and corresponding number of beads that were used to produce the calibration curve. 24

Chapter 5 Conclusions

Table 5.1 The transcriptional parameters of Pol I and Pol II 90

Chapter 1

Introduction

1.1 The Tethered Particle Motion technique (Tethered Particle Microscopy)

Conventional biochemical experiments have provided remarkable insight into the structural and mechanistic details of many biomolecules. However, in this type of studies, it can be difficult to obtain information on sub-populations and intermediates, because ensemble averaging obscures transient behaviors [1]. Conversely, single molecule experiments are designed to reveal the state or the position of individual molecules for a sufficient amount of time to observe biologically important molecular heterogeneity in conformational dynamics, molecular interactions, or intermediate steps of reactions.

Almost twenty-five years after the first application of a single molecule technique to the study of RNA polymerase activity [2], single molecule approaches are recognized for their tremendous power for biological investigations. With the implementation of technical advances, new single molecule techniques have been developed and early ones have been improved [3]. The detailed information that these techniques provide about biological processes, structures and function makes them widely applicable to the study and understanding of a variety of problems ranging from development of cancer therapeutics, characterization of molecular mechanisms, and detection of signaling pathways.

Tethered Particle Motion (TPM) is a simple, convenient and elegant technique compared to other single molecule techniques [4]. It is an optical method which allows monitoring of the dynamic properties of the sample, but avoids its mechanical

manipulation [5] and the application of external forces. Most commonly, TPM experiments involve monitoring changes in the length of a nucleic acid molecule (DNA or RNA) labeled at one end with a sub μm -sized bead and anchored to the surface of a microscope flow chamber at the other end [2, 5]. Therefore TPM is well suited to observe protein-induced changes in nucleic acid molecules conformation, like looping, condensation, or changes in the intrinsic elastic properties of the nucleic acid molecule due to soluble proteins, ionic strength.

The bead that reports the motion of the biomolecule can diffuse freely in a limited volume, which is constrained by the tethering polymer. A charged-couple device (CCD) records the motion of the bead for different time intervals. Then the bead positions are calculated by an appropriate single particle-tracking (SPT) algorithm. When the positions are analyzed, they indicate a restricted motion, which is a function of the contour length of the tether. Changes in tether length result in changes in the amplitude of the restricted motion (excursion value).

One of the main characteristics and advantages of TPM over other single molecule techniques is the absence of any externally applied force, which may perturb interactions between DNA and other molecules of interest [6]. For instance, single molecule experimentation has revealed that external loads of increasing magnitude slow down and eventually inhibit the activity of DNA-processing enzymes.

1.1.1 TPM Experimental Setup

Even though there may be different versions of TPM microscopes, a typical setup consists of three main elements: An optical microscope, an imaging device and a

computer. The microscope is needed to make the sample visible by magnifying it and differentiating it from the background. TPM has been implemented using differential interface contrast (DIC) microscopy [2], bright field microscopy [7], and more recently dark field microscopy [5].

Generally, a CCD video camera is used to acquire images of the sample [8]. The images may be directly transferred to a computer, perhaps via a frame grabber card. Motions of the reporter beads are analyzed using particle tracking algorithms. The position of tracked beads may be found with an accuracy of 10 nm [9], and recently, with an accuracy of 3 nm by using darkfield microscopy and nano gold particles [5]. Following that routines are used to correct for any possible drift. The drift-free positions of beads in sequential images are then analyzed to form two-dimensional distributions. Finally, a symmetry test is applied to the distributions to discard beads tethered by more than one molecule, or beads that transiently stick to the surface.

1.1.2 Experimental protocol for TPM experiments

In order to run a TPM experiment, the tether of interest, which is usually DNA, must be produced using the polymerase chain reaction (PCR) using a template plasmid and appropriate primers. Labeled primers are used to immobilize the DNA on the micro chamber surface and/or label it with a reporter bead. Common labels for specific attachment are biotin and digoxigenin. There are three different types of TPM experiments that one can envision depending on the biological question to be addressed; they are summarized in the **Figure 1-1**.

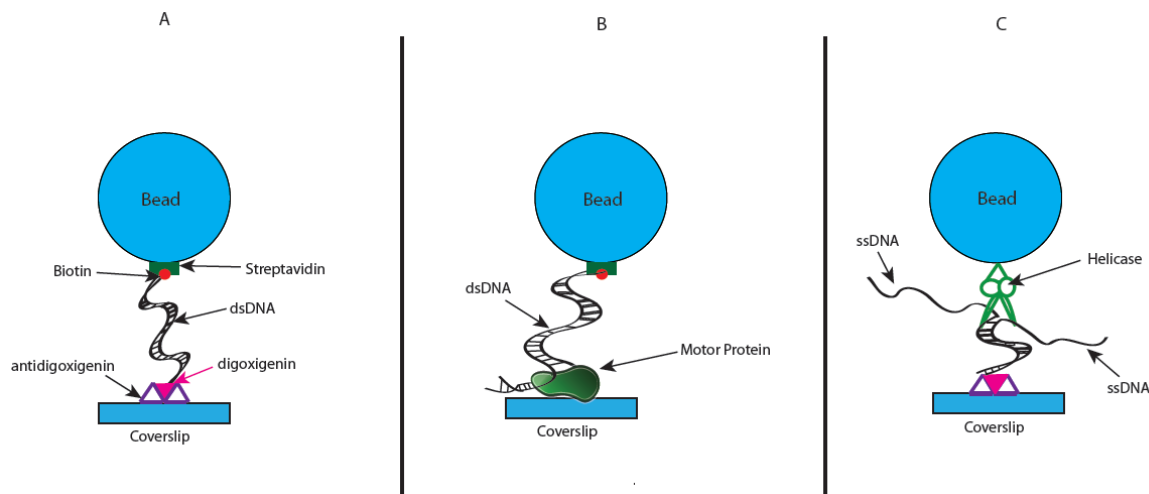


Figure 1-1 Different experimental design for TPM assays. (A) The bead is attached to the DNA tether by either a biotin or a digoxigenin label on the 5' end of the DNA. The bead is coated with streptavidin or anti-digoxigenin to match the label at one DNA end. Conversely, the glass surface is treated with either streptavidin or anti-digoxigenin to attach the other end of the DNA. This configuration is suitable for examining the conformational change of a DNA tether induced by enzyme protein, such as transcriptional regulators. (B) A motor enzyme that is bound to a DNA fragment is nonspecifically attached to the surface. The other end of the DNA is labeled with a bead. This configuration is suitable to study the enzyme activity on DNA. (C) DNA is immobilized on the surface by digoxigenin –anti- digoxigenin conjugation. A biotin-labeled enzyme is attached to the streptavidin coated beads. This configuration is ideal to characterize the activity of DNA helicases. Image was reproduced from [10].¹

1.1.3 TPM Measurements

TPM experiments are performed in aqueous environments; therefore the bead attached to the DNA exhibits Brownian motion. Since the attachment of the other end of the DNA is fixed either to the surface of the microscope flow-chamber by specific interactions or by an enzyme, the excursion of the bead is restricted. The volume of

¹ This figure is copyrighted by Springer and used here with the copyright permission license 3484281476990

confinement is defined by the bead size and the effective tether length, which is influenced by the ionic strength of the solution [11]. Therefore, calibration curves are necessary to relate the observable excursion of the bead to the known tether contour length. Subsequently, in order to study the activity of proteins on nucleic acids, TPM experiments should be run keeping the bead size and the buffer condition constant and equal to those of the calibration curve. Part of this study was consisted in generating calibration curves in conditions that were relevant to experiments performed in the lab.

Another parameter that needs to be considered carefully is the time in which tethered beads span the entire volume of confinement. This time needs to be determined experimentally, and depends on the ionic condition of the solution, the tether length and the bead size. Therefore, the excursion value, ρ , which is the measurable two-dimensional projection of the Brownian motion of the bead, is averaged over a minimum time span to determine any tether length changes.

The formula which is generally used to calculate the ρ value is shown in Equation 1.1 [4];

$$\langle \rho \rangle = \langle \sqrt{(x - \langle x \rangle_t)^2 + (y - \langle y \rangle_t)^2} \rangle_t \quad \text{Eq. 1. 1}$$

The values $\langle x \rangle_t$ and $\langle y \rangle_t$ define the center of the attachment that is found by averaging the x and y coordinates over a time interval, t .

1.2 RNA Polymerase

Figure 1-2 depicts the central dogma of biology, which explains the fundamental steps involved in protein synthesis, and highlights the role of RNA polymerase in this process.

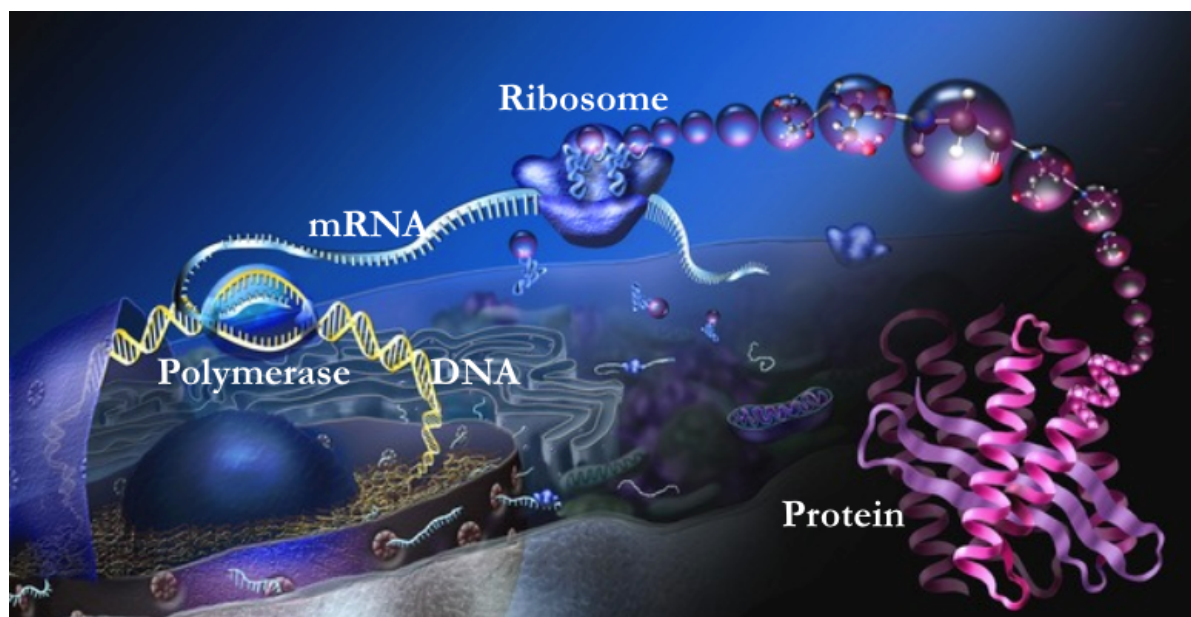


Figure 1-2 An illustration of the central dogma. Reactions involved in protein synthesis. The genetic code is read by RNA polymerases and the corresponding messenger RNA (mRNA) is produced. This mRNA chain is read by ribosome and converted to amino acid chains that form the primary structure of proteins. Reproduced from the digital painting of Nicole Rager Fuller, Courtesy: National Science Foundation.

Protein synthesis begins on the DNA with a unique enzyme, RNA polymerase which carries out transcription. During this process, the information encoded in one of the two DNA strands (the genetic code in A, T, G, C nucleotides) is read by RNA polymerase and a complementary form of the DNA template chain is produced, called messenger RNA, or mRNA. mRNA is the code read by the ribosome, the molecular

machinery which actually synthesizes protein synthesis.

There are two other forms of RNA in the cell: Transfer RNA (tRNA) and ribosomal RNA (rRNA). Transfer RNA (tRNA) coordinates the insertion of amino acids into the protein-synthesizing ribosome, to elongate the protein chain. Ribosomal RNA, rRNA, instead is the major component of the ribosome. Both tRNA and rRNA are called non-coding RNAs since they are actively involved in the process of protein production that is also called translation, but they do not provide the code for protein synthesis.

1.2.1 Types of RNA Polymerases

RNA polymerases are found in every species including viruses [12]. In bacteria, there is only one enzyme responsible for all the transcription activity, RNAP. Shortly after the discovery of RNA polymerases in 1960 [13], it was also found that RNAP includes a regulatory subunit, called sigma factor, that aids the selection of the sites for the initiation and the termination of transcription.

Unlike prokaryotic cells, the eukaryotic cells have a more complex mechanism for RNA synthesis [14]. First of all, there are multiple forms of RNA polymerases in eukaryotes [15]: RNA polymerase I (Pol I), RNA polymerase II (Pol II) and RNA polymerase III (Pol III) [16], each of which transcribes different specific RNAs. Pol II transcribes the protein coding genes and produces mRNA [17]. Pol I transcribes ribosomal RNA [18] and Pol III mainly synthesizes transfer RNA [19], but also some of the short rRNA. Most research thus far has been focused on characterizing the structure and activity of Pol II. Recently, single molecule studies revealed the kinetic

mechanism of Pol II [20, 21].

1.2.2 Transcription by RNA Polymerase I

Transcription can be divided into three main stages; initiation, elongation and termination. In the case of Pol I, initiation is the formation of the Pol I-DNA complex on the promoter region of the ribosomal DNA (rDNA). Initiation requires Pol I to recruit several transcription factors. Upstream activation factor (UAF) binds the upstream control sequence on the DNA [22]. TATA binding box (TBP) binds to the TATA region on the DNA. TBP facilitates the activity of the other eukaryotic RNA polymerases as well [23, 24]. The so called core factors, CF, consist of the Rrn6, Rrn11, and Rrn7 proteins that bind to TBP, Pol I and Rrn3p [25]. Lastly, Rrn3p binds to Pol I to enhance the stability of the Pol I-DNA complex [24]. Since Pol I lacks a domain for the identification of the rDNA gene, the auxiliary transcription factors described above are critical for Pol I initiation.

After forming a “closed complex” at the rDNA promoter, Pol I forms an open complex in which the two strands of the DNA are separated for approximately 13 bp. This is referred to as the transcription bubble. During each step of the elongation process, the enzyme adds a new nucleotide to the 3' end of the nascent RNA chain complementary to the 3' to 5' strand of the DNA template. After Pol I leaves the promoter, the initiation factors remain associated with the rDNA to facilitate the transcription of the same DNA template by another Pol I molecule.

When Pol I reaches the termination site at the end of the rDNA, a termination

factor binds and bends the DNA. This process forces Pol I to pause and finalize the NTP addition to the RNA transcript [26]. Then Pol I closes the transcription bubble and dissociates from the rDNA.

1.2.3 Structure of RNA Polymerase I

Pol I is composed of fourteen subunits as shown in **Figure 1-3**, five of which are identical to the other eukaryotic RNA polymerases. The identical subunits (Rbp5, Rbp6, Rbp8, Rbp10 and Rbp12) form the catalytic core of the enzyme. Another set of five subunits (A190, A135, AC40, AC19, AC12.2) have homologs in Pol II. Two other subunits (A14 and A43) have counterparts in Pol II. Finally, there are two subunits (A49 and A34.5) that are specific to Pol I [27]. Recently, the crystal structure of *Saccharomyces cerevisiae* Pol I has been resolved shedding light on the functional similarities between Pol I and the other polymerases [28].

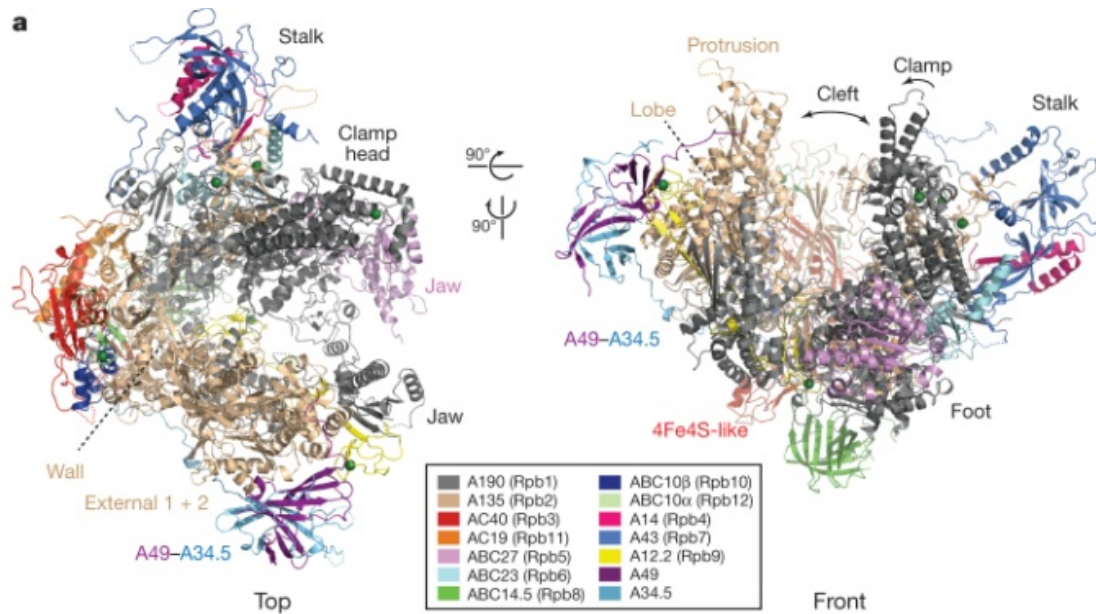


Figure 1-3 The crystal structure of the 14 subunit-Pol I from *Saccharomyces cerevisiae*. The figure is reproduced from Fernández-Tornero *et al.* [28].²

1.3 Motivation and Hypothesis

Pol I is uniquely responsible for the synthesis of the three largest rRNA species (28S, 18S, 5.8S) in eukaryotic ribosomes. Multiple studies over many years have demonstrated that ribosome synthesis is energetically costly for cells and directly connected to the rates of cell growth and proliferation [29]. Despite this connection to cell proliferation, the details of Pol I transcription remain poorly understood. Several recent findings suggest that transcription elongation by Pol I may deserve more thorough characterization. In 2007, the Nomura lab showed that selective impairment of Pol I transcription elongation results in rampant defects in the assembly of the ribosome [30]. Thus, transcription elongation by Pol I is functionally coupled to

² This figure is copyrighted by Nature Publishing Group and used here with the copyright permission license 3483691044778

functional translational machinery. Furthermore, a recent study from the Schneider and Kaplan labs discovered opposite phenotypes of identical mutations in highly conserved positions in the active core of Pols I and II [31]. The authors concluded that these enzymes have evolved unique elongation properties, perhaps to better suit each enzyme's unique cellular roles. In addition, the Cramer and Mueller labs recently solved high resolution crystal structures of yeast Pol I and found that the enzyme is dramatically different from Pol II in a number of critical domains [28, 32]. All of these data suggest that the transcription elongation properties of Pol I are unique and directly connected to cell viability and underscore the importance of a closer investigation of elongation by Pol I.

Pol I has also drawn interest as a potential target for anti-cancer chemotherapy [33]. Recent work from a number of labs suggests that developing a clear understanding of Pol I and its regulation may hold considerable clinical value [33, 34]. Based on the knowledge that ribosome synthesis rates are proportional to growth rate, a number of groups have identified molecules that directly inhibit transcription by Pol I. Both *in vitro* and in pre-clinical animal models, inhibition of transcription by Pol I results in selective inhibition of tumor cell growth [33, 34]. Thus, the therapeutic potential for inhibition of Pol I is high and a deeper understanding of Pol I transcription is warranted.

In this dissertation, a new method is presented, that allows single molecule transcriptional elongation by Pol I to be examined in real time. The assay employs promoter- and factor-dependent transcription initiation from the native promoter for Pol I. I assembled halted transcription elongation complexes on a template that carried

an epitope that could be linked by a polystyrene microsphere. Transcription elongation altered the length of the bead tether and could be monitored using TPM analysis. In order to overcome challenges presented by the low tethering efficiency of active elongation complexes, multiplexed tethered particle instrument was developed, so that it can now track hundreds of complexes at the same time. With this approach, a pause-free velocity for Pol I was observed that approached the values estimated for *in vivo* conditions from electron microscopy studies [35]. Furthermore, the frequent and non-random pausing by the polymerase was determined. Finally, and most surprisingly, under these conditions it was shown that only a small fraction of Pol I elongation complexes reached the end of the DNA template. Thus, Pol I is not processive *in vitro*, despite its exceptional processivity in living cells. Taken together, these data emphasize the utility of single molecule methods for describing the kinetics of transcription by Pol I, and suggest that *in vivo* one or more additional factors enhance processivity and reduce pausing of the enzyme.

To summarize, Chapter 1 contains background information about the TPM technique and Pol I. Chapter 2 explains the importance of the TPM calibration experiments that contributed and gave detailed information about the DNA sample and chamber preparation. Chapter 3 describes the development of the multiplexed TPM setup, its advantages over the conventional TPM methods and illustrates its application to the characterization of DNA wrapping by gyrase. Chapter 4 describes the preparation of stalled Pol I-DNA complexes, and focuses on the characterization of elongation by Pol I. Chapter 5 presents the conclusions of this dissertation.

Chapter 2

Calibration of Tethered Particle Motion³

³ This work was published in Biophysical Journal (2014, Vol. 106.2, Page 399-409) by © Elsevier

2.1 Introduction

Measurements carried out using the TPM technique are affected by the bead size, the tether length, the intrinsic properties of the DNA and the buffer condition. Segall *et al.* in 2006 investigated the effect of the bead size on the excursion value. Han *et al.* in 2009 varied both the DNA tether length and the bead size to explore the influence these parameters have on the motion of the bead [11, 36]. It is also known that the persistence length of the DNA varies with the change of the ionic condition [37]. Therefore, each new buffer condition necessitates a calibration curve in order to relate the excursion values to the DNA tether length. For this reason, an accurate calibration curve was recorded in order to interpret the transcription TPM experiments.

Furthermore, according to previous calibration data reported in the literature, both average and root mean square excursions are more accurate for shorter DNA fragments and become less sensitive, with a higher standard deviation, for DNA tether lengths of 3 kbp or longer. This is not a serious impediment for experiments where the tether length may vary between distinct values (DNA conformational states) widely separated in the range below 3 kbp. However, the uncertainty on the tether length of longer DNA fragments can limit the analysis of elongation or pausing events during transcription [38, 39]. Fortunately, our collaborator, Dr. Dunlap, realized that the dependence of the mean square excursion values on DNA tether lengths is linear. Then the calibration values were recorded for DNA tethers of known length in the experimental conditions of interest for my experiments, and assessed the accuracy of the mean square excursion calibration. The calibration curves became part of Figure 4 and Supplementary Figure 6 in Kumar *et al.* [40].

2.2 Materials and Method

2.2.1 DNA Preparation

DNA plasmids were used as templates, and DNA fragments were amplified using polymerase the chain reaction (PCR) with the biotin and digoxigenin labeled primers listed in the **Table 2.1** (Integrated DNA Technologies Inc., Coralville, IA or Invitrogen, Life Technologies Corporation, Carlsbad, CA), *Taq* polymerase (New England BioLabs Inc., Beverly, MA) and deoxyribonucleotides (Fermentas-Thermo Fisher Scientific Inc., Waltham, MA). The PCR products were purified using Qiagen purification kits (Qiagen, Germantown, MD). The length of the different DNA fragments was confirmed by gel electrophoresis.

Table 2.1 DNA tether lengths for calibration experiments

Length	Plasmid	Forward Primer	Reverse Primer
225 bp	pDL1051 [41]	5'-CGCAATTAATGTGAGTTAGCTCACTCATTAGGCACCCCAGGC-3'	5'-CCGCTCATGAGACAATAA-3'
590 bp	pDL611 [42]	5'-AAGAGTTTGTAGAAACGCAA-3'	5'-TATGCCCGAGAAGATGTT-3'
1064 bp	pDL1051 [41]	5'-AAGGTA ACTGGCTTCAGC-3'	5'-CCGCTCATGAGACAATAA-3'
1555 bp	pDL944 [43]	5'-CGCAATTAATGTGAGTTAGCTCACTCATTAGGCACCCCAGGC-3'	5'-GCATTGCTTATCAATTTGTTGCAACGAACAGGTCACTATCAGTC-3'
1898 bp	pDL186 [43]	5'-CGCAATTAATGTGAGTTAGCTCACTCATTAGGCACCCCAGGC-3'	5'-GCATTGCTTATCAATTTGTTGCAACGAACAGGTCACT-3'ATCAGTC-3'
2974 bp	pDL1051 [41]	5'-AAGGTA ACTGGCTTCAGC-3'	5'-GCATTGCTTATCAATTTGTTGCAACGAACAGGTCACTATCAGTC-3'

2.2.2 Chamber Preparation

The chamber was prepared following steps similar to those described by Dunlap *et al.* 2011 [8]. In brief, coverslips with size 22 X 22 mm (Fisherbrand, catalog number 12548B) , and 50 x 24 mm (Fisherbrand, catalog number 12545F) were cleaned with a solution of laboratory detergent, and then were rinsed copiously with tap water followed by a few rinses in de-ionized water. Then the coverslips were rinsed again with ethanol and submerged in ethanol in a closed container. Two strips of double-sided tape were cut to the same length as the 22 mm coverslip and width of approximately 2 mm. The two strips were placed parallel to the long sides of the 50 mm coverslip to eventually glue in place the 22 mm coverslip. A thin line of high vacuum grease was deposited just inside the length of the double-sided tape. The 22 X 22 mm coverslip was carefully placed on top of the 50 X 24 mm coverslip. The edges of the coverslip were gently pressed to ensure adhesion. A rectangular channel, or flow-chamber, was thus created which held approximately 25 μ l of liquid. Then the chamber was flushed twice with 200 μ l of phosphate buffer saline (PBS) buffer (10 mM phosphate, 150 mM sodium chloride, pH 7.4) by depositing a droplet of buffer at the opening of the channel and allowing capillary action to draw in the first volume. Then, more buffer solution was added to the opening of the chamber and introduced by wicking the solution in the chamber into a tissue at the outlet the chamber. All subsequent buffer exchanges were similarly performed. Then, 40 μ l of 40 μ g/ml of Bio-BSA in PBS were introduced into the chamber and incubated at least 2 hours at room

temperature or overnight at 4 °C. Then, 100 pM of DNA were incubated with polystyrene microspheres (anti-dig-coated, 240 nm radius, Indicia, France) in a 1:10 molar ratio for no longer than 10 minutes to avoid producing beads with more than one DNA molecule attached. After incubation, the chamber was flushed with at least two volumes of TR buffer with 0.5mg/ml α -casein (Sigma Aldrich, C6780 catalog number, St. Louis, MO) and incubated for 5 minutes to passivate the surface. Then, 50 μ l of 50 μ g/ml streptavidin were added to the chamber and incubated for 1 hour. Afterwards, the chamber was flushed twice with TR buffer, and then the DNA-bead solution was gently drawn into it and incubated for 30 minutes. Finally, the chamber was gently flushed with 4 -5 volumes of the TR buffer.

2.2.3 Particle tracking, Data acquisition, and Instrumentation

All TPM measurements were performed at room temperature. A Leica DM LB-100 microscope (Leica Microsystems, Wetzlar, Germany) with oil-immersion objectives (100X, NA 1.2–1.4 or 63X, NA 0.6–1.4), as shown in **Figure 2-1**, was used to observe tethered beads with differential interference contrast (DIC) optics. DIC has a high signal/ noise ratio and allowed 30 ms exposures with no significant blurring due to the motion of the beads [36, 44]. The instrument and analysis were described in detail in Kumar *et al.* 2014 [40].



Figure 2-1 A representative optical setup for tethered particle microscopy with DIC optics. Image was reproduced from [8].

“The user interactively selects single particles (small and symmetric) with circular ranges of motion by circumscribing them in a rectangular region of interest. Interlaced video at 25 Hz from a CV-A60 CCD camera (JAI, Copenhagen, Denmark) digitized with an IMAQ PCI-1409 frame grabber (National Instruments, Austin, TX) was analyzed in real time using custom LabView (National Instruments) routines. The position of each bead was determined in each video frame and the time series of xy coordinates was stored in a text file. In DIC, the bead image is made of two juxtaposed semicircles, one bright and one dark. The centroids of both semicircles were averaged to establish the bead position. The routine accurately tracks up to 30 beads in real time on a personal computer with 512 MB of 133 MHz RAM and an AMD Sempron 3100+ processor operating at 1.8 GHz. Further details about the instrumentation and the real-time analysis are available [4, 40].”

2.2.4 Data Preprocessing and Drift Calculations

“Data was recorded from fields of view with more than 3 beads. Only time series for tethered beads that did not stick directly to the surface during observation were used for the drift calculations. A 40 s moving average (center of mass) for the selected beads in a video frame was calculated and a vector which represents the drift motion due the vibrations of experimental setup was subtracted from all the xy coordinate vector for the position of each bead to remove the low-frequency drift without reducing the independent Brownian motion of the bead [4, 36]. Data from time intervals in which the bead transiently stuck to the surface were deleted. Time series lasting more than a minute were used in the next step of data preprocessing [40].”

2.2.5 Symmetry Test

Beads that are attached to the surface by only one DNA tether will exhibit symmetrical excursions about the anchor point, whereas those attached to two or more widely separated points will not. Therefore, the symmetry of the drift-corrected beads was checked in two qualitative and one quantitative ways. First, the user judged whether or not the scatter of xy positions of the drift-corrected beads was circular as shown in **Figure 2-2-(A)**.

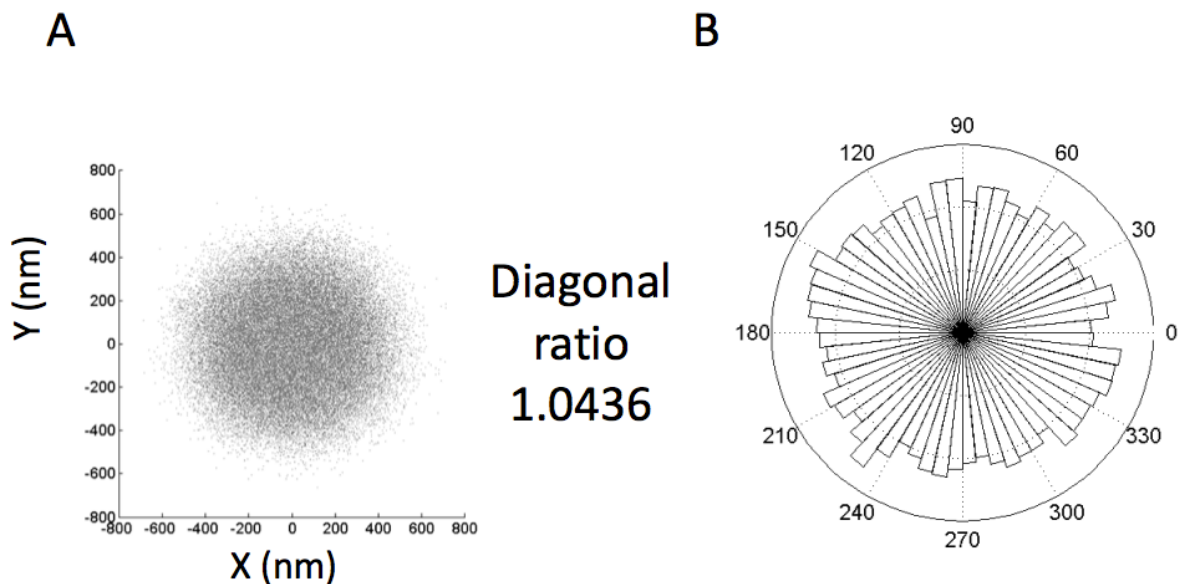


Figure 2-2 Symmetry of bead motion. A) In 400 seconds a drift-corrected bead of 240 nm radius attached to a 2211 bp DNA tether was observed at these xy positions. B) A radial histogram of the angular coordinates for the same positions allowed judgment of whether or not the bead equally sampled all sectors (6 degrees) of the available hemisphere. The ratio of major to minor diagonals was 1.0436 [40].

“Second, a radial histogram of the angular coordinates was displayed for the user to judge whether or not the bead equally sampled all sectors of the available hemisphere (**Figure 2-2-(B)**). Third, a covariance matrix of the xy positions was constructed, and the ratio of longest to shortest diagonal was determined by calculating the square root of the ratio of the eigenvalues of the covariance matrix [36, 45]. Previously, Han *et al.* accepted beads with a diagonal ratio ≤ 1.1 . In this study, only the beads with a diagonal ratio < 1.07 were included for further analysis [36, 40].”

“To exclude beads attached to two or more DNA tethers that passed the symmetry test and small clusters of beads on a tether, and to select a set of beads of the same size attached to single DNA tethers, Nelson *et al.* rejected beads with distributions of excursions (ρ distributions) that were unlike the majority [4]. Here,

the JMP routine from SAS (JMP, Version 9, SAS Institute, Cary, NC) was used to hierarchically cluster ρ , $(\sqrt{x^2 + y^2})$, distributions using a centroid method by assigning them to the nearest cluster center to reject outliers and select beads with similar ρ distributions as shown in **Figure 2-3** [40].”

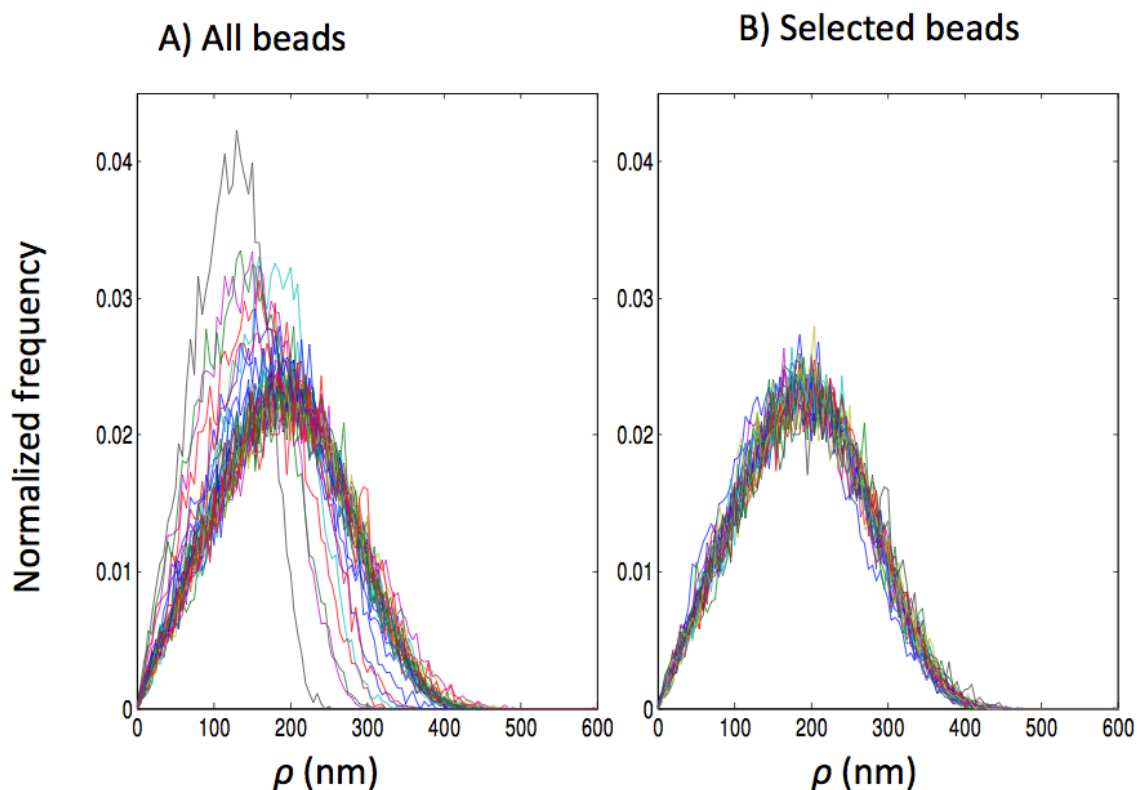


Figure 2-3 Selection of beads based on ρ distributions. (A) Normalized frequency distributions of the observed excursions, $\rho = \sqrt{x^2 + y^2}$, in one field of view were plotted for beads with 160 nm radii attached to DNA tethers of 1093 bp. (B) Beads exhibiting similar excursions were selected by hierarchical clustering of frequency distributions using a centroid method [40].

2.3 Results

The calibration experiments were performed with different DNA tether lengths: 225, 590, 1064, 1555, 1898 and 2974 bp. These lengths were chosen to represent the

range of DNA tether lengths during a typical transcription elongation experiment. Several fields of view from the same chamber were recorded and analyzed. After bead selection (see section 2.2.5), the total number of beads used for the calibration curve was as shown in Table 2.2.

Table 2.2 DNA tethers and corresponding number of beads that were used to produce the calibration curve.

	240 nm (radius) beads
	TR buffer
DNA tether length (bp)	Numbers of beads
225	15
590	8
1064	24
1555	20
1898	16
2974	19

2.3.1 Mean Square Excursion

Efforts have been made to simulate the tethered motion of beads, however no analytical solution has been found to describe it [46]. Therefore, a new calibration was needed for each new buffer condition. In order to obtaining a calibration curve, different calculations of mean excursions were used. Previously a moving average of ρ was calculated using the Equation 2.1 [5, 8];

$$\langle \langle \rho \rangle_t = \langle \langle \sqrt{(x - \langle x \rangle_t)^2 + (y - \langle y \rangle_t)^2} \rangle_t \rangle_t \quad \text{Eq. 2.1}$$

more recently other researchers used the root mean square of ρ using the Equation 2.2 [47-51]:

$$\zeta_{\text{rms}} = \sqrt{\langle \rho^2 \rangle_t} = \sqrt{\langle ((x - \langle x \rangle_t)^2 + (y - \langle y \rangle_t)^2) \rangle_t} \quad \text{Eq. 2. 2}$$

Even though both calibration values for $\langle \rho \rangle$ and ρ_{rms} were useful for converting the excursions to the DNA tether lengths, both methods lose sensitivity with increasing DNA tether length because of the fewer angular confirmations when point of linkage is close to the surface [11]. **Figure 2-4** depicts the ρ_{rms} values for different bead and DNA tether sizes. The curve shows decreasing changes in ρ_{rms} values as the DNA tether length increases. This undermines sensitivity of the calibration at longer tether lengths.

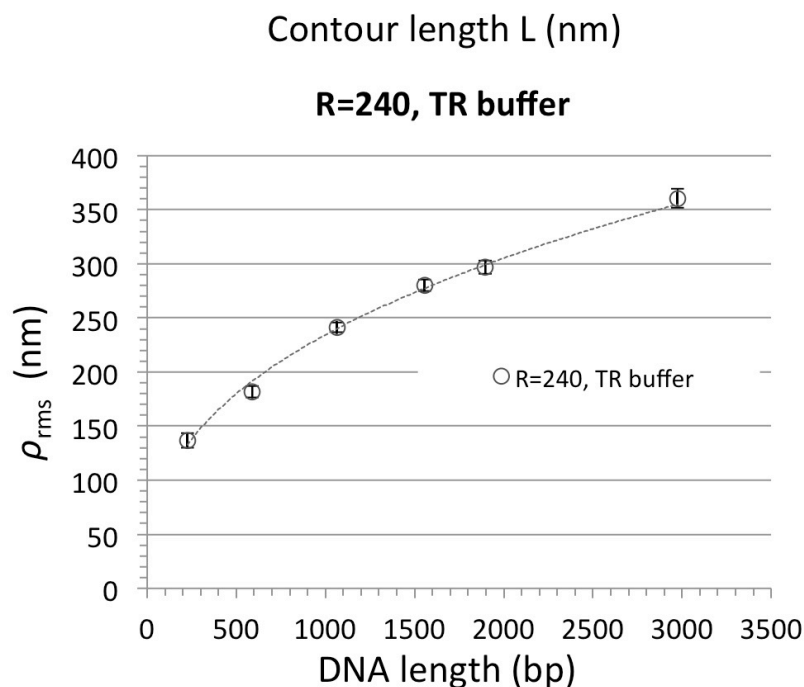


Figure 2-4 Calibration of root-mean-square excursion versus DNA contour length. Excursions of tethered beads (radii of 240 nm) in TR buffer were calculated using the equations 2.1 and 2.2. The data are for 240 nm radii beads in TR buffer (20 mM Tris-acetate, pH 7.9, 2 mM DTT, 100 mM potassium glutamate, 8 mM magnesium acetate) (\circ). Connecting curves linking similarly sized beads in identical buffers are shown as guides. Error bars are standard deviations of the excursions for ensembles of identically assembled tethered beads.

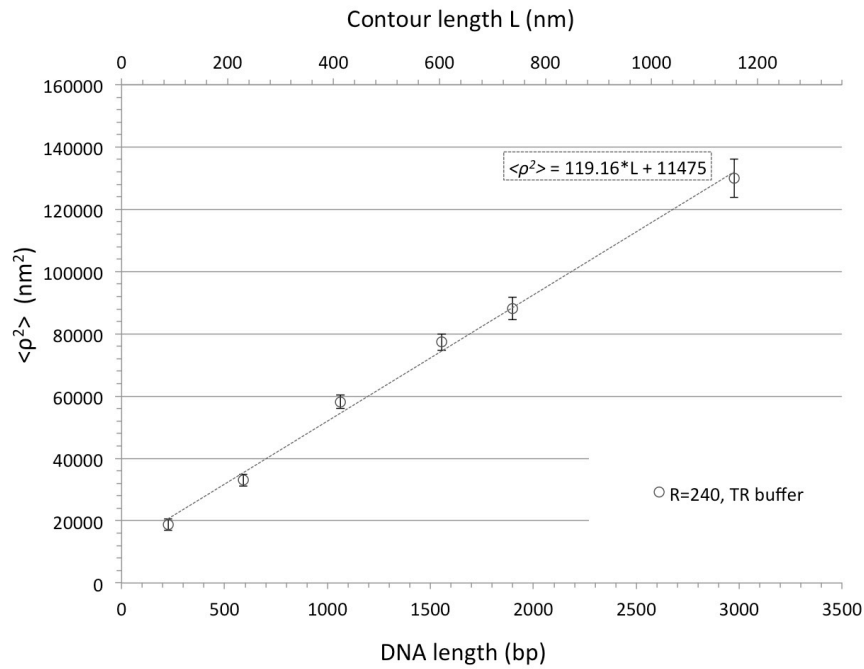


Figure 2-5 Calibration of mean-squared excursion versus DNA contour length. Mean-squared excursion values of tethered beads with 240 nm radii beads in TR buffer ($\langle \rho^2 \rangle = 119.16 * L + 11475$, \circ). Error bars indicate standard deviations of the time-averaged excursions measured for an ensemble of symmetrically moving tethered beads with closely clustered values.

The mean square excursion values were also calculated for the different DNA tether lengths according to:

$$\langle \rho^2 \rangle_t = \langle ((x - \langle x \rangle_t)^2 + (y - \langle y \rangle_t)^2) \rangle_t \quad \text{Eq. 2.4}$$

in order to test the dependence of $\langle \rho^2 \rangle$ values on DNA tether lengths. **Figure 2-5** shows a linear relationship.

2.4 Conclusion

Due to the lack of an analytical expression that relates the excursion of the bead to the tether length in TPM experiments, a calibration curve must always be obtained. Here, it is shown that because of the linear dependence of the mean of squared excursion values on DNA tether lengths, it is more practical to build calibration curves based on this parameter.

Chapter 3

Multiplexed Tethered Particle Motion

3.1 Introduction

Since TPM is a powerful technique with many potential applications, it has been the object of intense study and optimization. Recently, Garini *et al.* proposed to use confocal microscopy to observe the excursion motion of the labeling bead in three-dimensions [46]. Other investigators have concentrated on trying to increase the throughput of the technique. For example, Salome *et al.* reported a method which allowed the observation of hundreds of immobilized complexes simultaneously [52]. With this improvement they reported the activity of T7 bacteriophage exonuclease enzyme which was previously examined only using bulk assays, because of the low processivity in single molecule experiments [52]. However, the equipment they developed to achieve such high throughput, including nanofabricated chamber assembly and either commercial or custom software are not easily available to many laboratories. In contrast, a similar level of simultaneous bead tracking, multiplexing, was achieved in a much simpler and less expensive manner in this study.

Multiplexed TPM was used mainly to perform Pol I transcription experiments. However, it was also tested with *E.coli* DNA gyrase, a type II topoisomerase enzyme. *E.coli* DNA gyrase adds negative supercoils to the DNA. It does that by wrapping a segment of DNA around gyrase's C-terminal domains (CTDs) prior to the cleavage and strand passage of an adjacent segment of the DNA (T-segment). The cleavage and strand passage activities require ATP but the wrapping event does not. In a tethered DNA, the wrapping and unwrapping events create a telegraphic length changes. Therefore, the wrapping activity of the gyrase can be observed by the monitoring the

changes of the excursion value of a bead tethered by DNA.

3.2 Materials and Methods

3.2.1 Sample Preparation for Transcription experiments

To characterize Pol I elongation by TPM, one can start with stalled complexes of Pol I and DNA obtained by adding only three of the four nucleotides. The probability of restarting a stalled Pol I-DNA complex in solution is close to 2% as reported in Aprikian *et al.* [53]. Details for the transcription complex can be found in Schneider *et al.* 2012 [54]. For the sample preparation, the DNA was amplified by polymerase chain reaction (PCR) using plasmid pNOY745 which includes a segment of the *Saccharomyces cerevisiae* rDNA gene. The amplicon was 2.5 kbp-long and consisted of 500 bp before, and 2 kbp after the promoter sequence. High fidelity DNA polymerase (Phusion, New England BioLabs Inc., Ipswich, MA) was used during the PCR reaction cycle with biotin and digoxigenin-labeled primers (Integrated DNA Technologies Inc., Coralville, Iowa). Labeled primers had the following sequences: 5'-tcactccaccaactgagaaacg and 5'-atggtgaaagttcctcaagaat. Silica-membrane based purification kits (Qiagen; Germantown, MD) were used to obtain the DNA templates from the PCR products. The lengths of the purified DNA templates were checked using gel electrophoresis.

RNA Polymerase I, Rrn3p, TATA binding protein (TBP) and core factor (CF) were kindly provided by the Schneider lab. Procedures for the purification of these enzymes were published by Schneider *et al.* 2007 [30]. Preparation of the single molecule assays

includes the following steps: First, a pre-initiation complex was assembled by mixing 0.5 pmol of DNA template, 0.3 pmol of CF, 0.3 pmol of TBP in 43.1 μ l of TR buffer complemented with 0.5 mg/ml α -casein, and waiting three minutes to allow binding of the enzymes on the template DNA. After three minutes, 0.25 pmol Pol I – Rrn3p pre-formed complex were added to the solution of DNA and co-factors and then incubated for additional ten minutes at room temperature in order to facilitate the formation of the pre-initiation complex. Then, two μ l of NTP mix, containing 10 mM of ATP, GTP, and UTP, were added to the pre-initiation complex and incubated for three minutes. At this point, the pre-initiation complexes should have progressed through initiation, and subsequently formed elongation complexes. At the 56th bp, the complex would stall due the absence of CTP.

Then, approximately 20 μ l of the stalled complexes were slowly added to the chamber, which was previously treated with anti-HA. Since the C-terminus of the A135 subunit of the Pol I complexes includes a 3-HA epitope, fifteen minutes of incubation facilitated the binding of Pol I to the chamber surface through the anti-HA:HA conjugation. Meanwhile 1 μ l of 480 nm radius, anti-dig coated beads (Indicia Diagnostics, Oullins, France) were diluted with 49 μ l of TR buffer and vortexed for 15 minutes to eliminate aggregates. Then, 400 μ l TR buffer were slowly added to the chamber to flush out the unbound complexes. Five minutes after flushing, 25 μ l of the bead mixture were added to the chamber and incubated for 15 minutes to facilitate the binding of the digoxigenin labeled DNA to the anti digoxigenin-coated bead surface. After incubation, the chamber was flushed slowly with 400 μ l of TR buffer and then placed on the microscope for imaging.

3.2.2 Sample Preparation for Gyrase wrapping experiments

The experimental setup is similar to that of the calibration experiments discussed in Chapter 2. The DNA was labelled with biotin at one end and with digoxigenin at the other end. The chamber was incubated with Biotin-BSA (40 $\mu\text{g}/\text{ml}$) overnight at 4°C. Then it was washed with 400 μl lambda buffer which contained 10 mM Tris-HCl (pH 7.4), 200 mM KCl, 5% dimethyl sulfoxide (DMSO), 0.1 mM ethylenediaminetetraacetic acid (EDTA), 0.2 mM dithiothreitol (DTT). Afterwards, it was treated with 50 μl of 50- $\mu\text{g}/\text{ml}$ streptavidin and incubated for one hour. Meanwhile, 2.5 μl of the 480 nm anti-dig coated beads were diluted with 47.5 μl lambda buffer and vortexed for 15 minutes. Then the 335 bp DNA (1 ng/ml) was added to the bead solution and incubated for 1 hour. The chamber was washed with 400 μl lambda buffer. Then 25 μl of bead-DNA solution were added to the chamber and incubated for 2 hours. After this incubation, the chamber was washed with the 400 μl lambda buffer and placed on the microscope stage to acquire control data for 5 minutes. Then, 40 μl of gyrase solution (0.2 μl *E.coli* gyrase, New England Biolabs (NEB), Ipswich, MA), with 39.8 μl lambda buffer) was added to the chamber and changes of the tether lengths were monitored.

3.2.3 Chamber assembly

For the chamber preparation, coverglasses (Fisherbrand, 50 x 24 mm, catalog number 12545F) and coverslips, with dimensions 22 X 22 mm (Fisherbrand, catalog number 12548B), were washed with soapy water and cleaned with deionized water.

Afterwards, they were stored in pure ethanol. The Flow chamber was assembled with double-sided tape spacers lined with vacuum grease to attach the coverslip to the cover glass (**Figure 3-1**).



Figure 3-1 Assembly of the chamber for TPM experiments. The chamber was prepared from high vacuum grease (grey) and double sided tape (blue) between two coverslips. The vacuum grease keeps the solution inside the chamber area. The double-sided tape glues the two coverslips together. The coverslips were washed with pure ethanol and dried with Kimwipes.

Once the chamber was built, it was flushed with nano pure water and then TR buffer. The final shape of the chamber is shown in **Figure 3-2**. Since the Pol I samples were labeled with HA tag, the immobilization on the glass surface was achieved by coating the chamber with anti-HA antibody (Monoclonal, Host: Mouse, Clone#: 12CA5, Abcam, Cambridge, MA). Coating was achieved by introducing a solution of the antibody, and incubating at least 2 hours at room temperature or overnight in a 4°C refrigerator. Then, the remaining solution was flushed with TR buffer supplemented with 0.5mg/ml α -casein (Sigma Aldrich, catalog number C6780) for surface passivation.

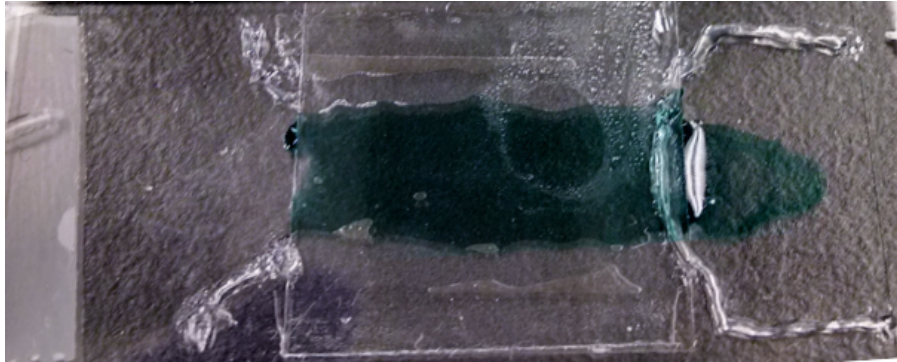


Figure 3-2 The assembled chamber on a microscope slide. A green dye was injected into the chamber to make the chamber channel visible in this image.

3.2.4 Optical Setup

A Leica DM LB2 upright microscope ((Leica Microsystems, Wetzlar, Germany) was used with a Leica 506287 oil immersion objective (63X, NA 1.4). A Leica Optivar lens (541 517 HC, 0.33X-1.6X) was used at 0.63X demagnification level with a CM-140GE video camera (JAI, Copenhagen, Denmark) to increase the field of observation. The components of the aforementioned system are shown in **Figure 3-3**. The total magnification of the field of tethered samples was 40X, which was sufficient for good digital resolution of the beads with 6-8 pixels per bead. The dark-field microscopy setup had an objective with 20X magnification. Up to 100 tethered particles were observed per field of view with random distribution of the tethers on the chamber surface.

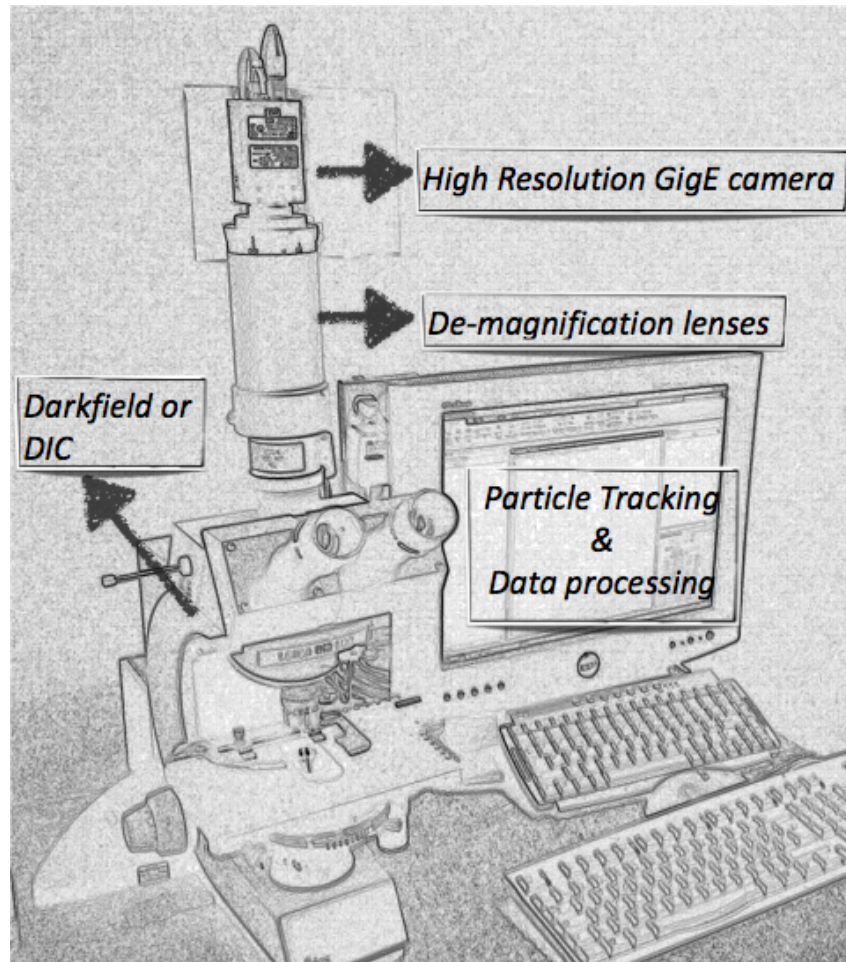


Figure 3-3 Multiplexed TPM setup. A DIC or dark field microscope was equipped with camera mount lenses (de-magnification) to reduce the magnification level. The 63X microscope objective was coupled with 0.63X de-magnification level that produced an effective 40X magnification of samples. A high-resolution camera was used for image acquisition and a quad core CPU computer was programmed to record the images and analyze the particles.

3.2.5 Hardware and Software

A camera with gigabit Ethernet (gigE) connection was used to transfer the acquired images with 1390 x 1040 pixel resolution to the computer at 30 frames per second. The frame rate with 30 ms exposure value was sufficient to observe the beads without

blurring due to the fast bead motion. In our tests, the images were streamed at 125 MB/s. To maintain high data rates, Cat 6e network cable was used to connect the camera to the computer. The computer system had the following specifications; AMD quad core CPU with 3 GHz frequency clock, 4 GB of DDR3 memory and 500 GB hard disk for operating system and software installations and a separate 2 TB 7200 rpm Western Digital Black series hard drive for video recording. The NI-IMAQ driver was coupled with Intel Pro 1000 series network adaptor to decrease the load of communication with camera on the CPU. In order to grab the acquired images, Labview with NI Vision Acquisition Software (National Instruments, Austin, TX) with NI-IMAQdx High Performance driver were programmed to capture, display and save the stream as uncompressed AVI video file.

The Matlab (MathWorks, Natick, MA) *VideoReader* class was used to access each frame by reading the video file. Meanwhile, the locations of the tethered beads were determined by playing the video file with an open source video player (VLC). Using the *imcrop* function of the image acquisition toolbox, each bead was selected and the region of interest around it was registered to the Matlab routine. Then, tracking of each bead inside the selected area was performed in consecutive frames. There are several methods for finding the locations of the bead each with some advantages and some drawbacks. In this case a recent tracking algorithm based on radial symmetry was implemented to track the tethered beads [55]. A nonlinear Gaussian tracking algorithm was also applied for the assessment of the accuracy of the radial symmetry method. The comparisons of the two methods are explained in the Results section.

3.2.6 Drift correction and bead selection

After the positions of the beads were obtained, a set of analyzes were applied to reveal the actual Brownian motion, as explained in Kumar *et al.* 2014 [40]. First, the mechanical drift was eliminated by subtracting the apparent motion of stuck beads. Then, a radial distribution of the positions was plotted to check the symmetrical behavior of the excursion in the XY plane as shown in **Figure 3-4**.

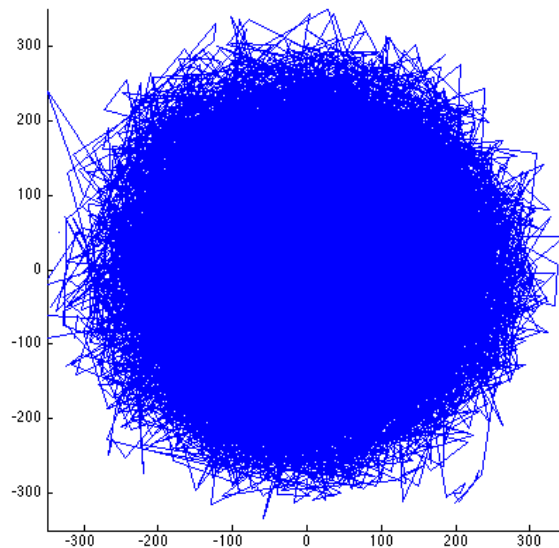


Figure 3-4 Circular excursion pattern of singly tethered beads. The drift free positions of the tracked bead were plotted to check the circular shape of the excursion. In case of multiple tethering, the shape should resemble that of an ellipsoid.

If the bead had more than one attachment, then the area it would cover in time would have the shape of an ellipsoid rather than a uniform circular area. Therefore, examining the circular shape of the radial distribution that is shown in **Figure 3-5** was useful to eliminate beads tethered by multiple DNA molecules. Then, the covariance

matrices of coordinates were calculated and beads that had a diagonal ratio smaller or equal to 1.07 were considered for the further analysis.

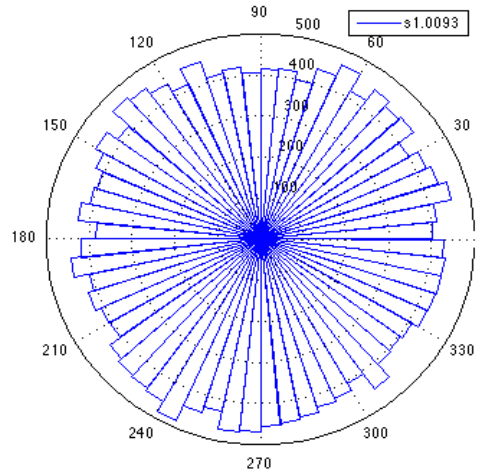


Figure 3-5 The angular distributions of bead positions. The circular shape in **Figure 3-4** does not definitively demonstrate a uniform distribution of the positions. However, an angular distribution plotted to confirm the uniformity of the positions inside the circle does. The covariance matrix was also calculated to check the symmetric shape of the bead positions. The beads with the values greater than to 1.07 were discarded and were not used for future analyze.

The data selected after drift correction were analyzed to calculate the mean square excursion values according to Equation 3.1:

$$\langle \rho^2 \rangle_t = \langle ((x - \langle x \rangle_t)^2 + (y - \langle y \rangle_t)^2) \rangle_t \quad \text{Eq. 3.1}$$

where x and y are the instantaneous coordinates and $\langle x \rangle_t$ and $\langle y \rangle_t$ are the coordinates of the point of attachment of the bead found by averaging the positions for $t = 4$ seconds.

3.3 Results and Discussion

The development of a multiplexed TPM was dictated by the low restart efficiency, 1-2%, of stalled Pol I-rDNA elongation complexes.

3.3.1 Accuracy of radial symmetry tracking

After imaging the complexes, the particles were tracked using radial symmetry and non-linear Gaussian fitting. Recently Parthasarati *et al.* established a method using the intensity gradients and tested the accuracy of the radial symmetry algorithm for images obtained from various microscopic techniques [55]. In this study, the approach that Parthasarati *et al.* developed has been altered specifically for the images that are obtained from our DIC microscopy and multiplexed TPM setup and the test for the accuracy has been done successfully. The intensity gradients on a pixel map of a representative DIC image are shown in **Figure 3-6**.

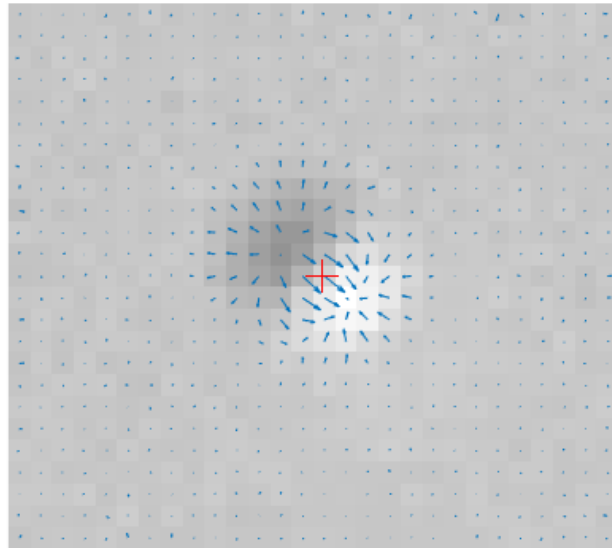


Figure 3-6 A representative DIC image and the intensity gradients. The gradient lines (blue arrows) were plotted according to their magnitude. The calculated center of mass was shown in red cross.

Since the DIC images consist of adjacent semi-dark and semi-bright spots, they are not symmetrical in all directions. However, a 45° orientation of the dark and the bright spots with respect to the Cartesian coordinates, achieves the equal distribution of the gradient lines that are centered to the bright and dark spots. Then, the point which minimizes the weighted sum of the squared distances to all the lines passing from the pixel centers and parallel to the gradient lines were calculated. Parthasarati *et al.* provided an analytic solution of the minimization problem for the symmetric images [55]. Although it is possible to restrict the contribution of the gradients outside of the region of a bead, it has a major disadvantage: this constraint needs to be re-evaluated for each magnification level and different bead sizes. In addition, it is safe to assume that the contribution of the noise is symmetrical, therefore the noise from different positions eliminate each other due to the symmetry.

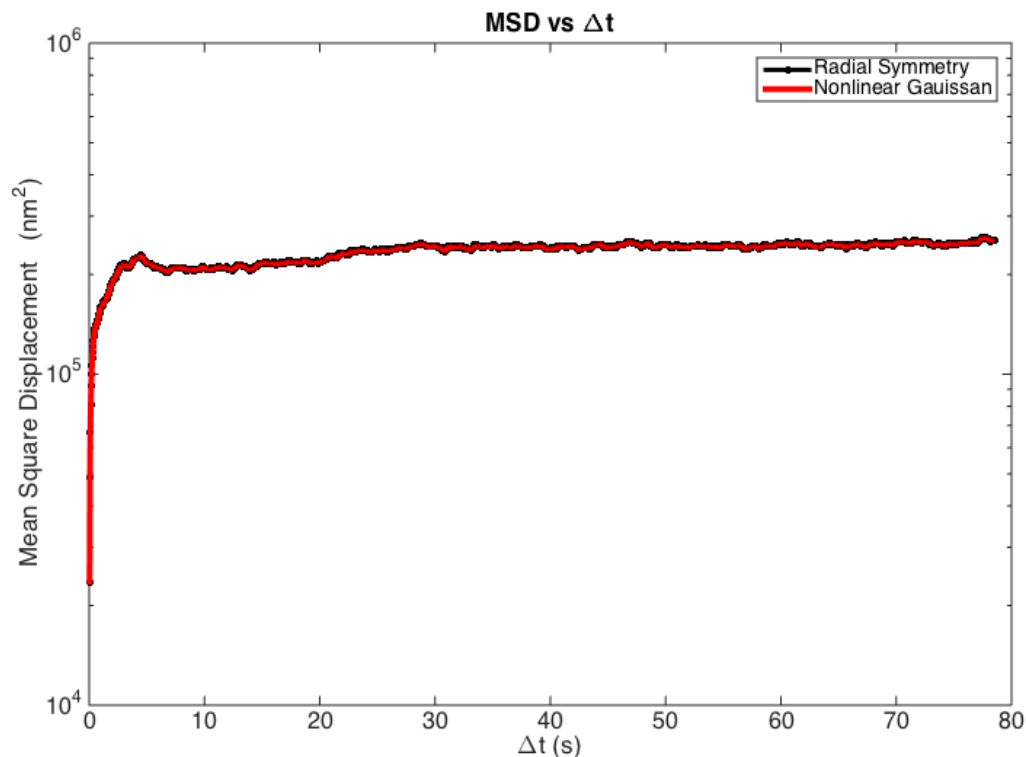


Figure 3-7 Comparison of the two tracking algorithms; non-linear 2-D Gaussian fitting (red line) and radial symmetry (black line). The mean square displacements were calculated using the Cartesian coordinates obtained by the two different algorithms. The plot shows that the results of two algorithms overlap. The Gaussian algorithm was known to be a precise, computationally intensive method, but the radial symmetry algorithm was attractive, because it is less demanding computationally (70X faster in our benchmarks). The results overlapped quite closely, so the non-linear Gaussian was plotted thicker to enhance visibility.

An assessment was made with the DIC microscope images. For comparison, a non-linear 2-dimensional Gaussian algorithm which gives high accuracy was used. The results obtained with this method and the radial symmetry approaches are shown in **Figure 3-7**. The differences of the tracking methods were compared by looking at the mean square displacement (MSD) [56]. Interestingly the curves obtained with the two different algorithms are very close to each other, even in the small fluctuations along the curves and even though the computational time required for the non-linear 2-D

Gaussian algorithm was 70 times longer than that for the radial symmetry algorithm.

3.3.2 Effect of Averaging Time

Figure 3-7 shows that the mean square displacement changes more in the first few seconds than in the rest of the curve. This behavior is related to the time required for the tethered bead to explore the accessible volume limited by the tether. Previous studies [36, 40] showed that 480 nm diameter beads require only four seconds to cover the maximum excursion volume. However, in our assays, the enzyme (Pol I) was attached to the surface instead of DNA as in the previous studies [57]. Therefore, the minimum time required to accurately establish the point of attachment of the beads was found for this new experimental condition.

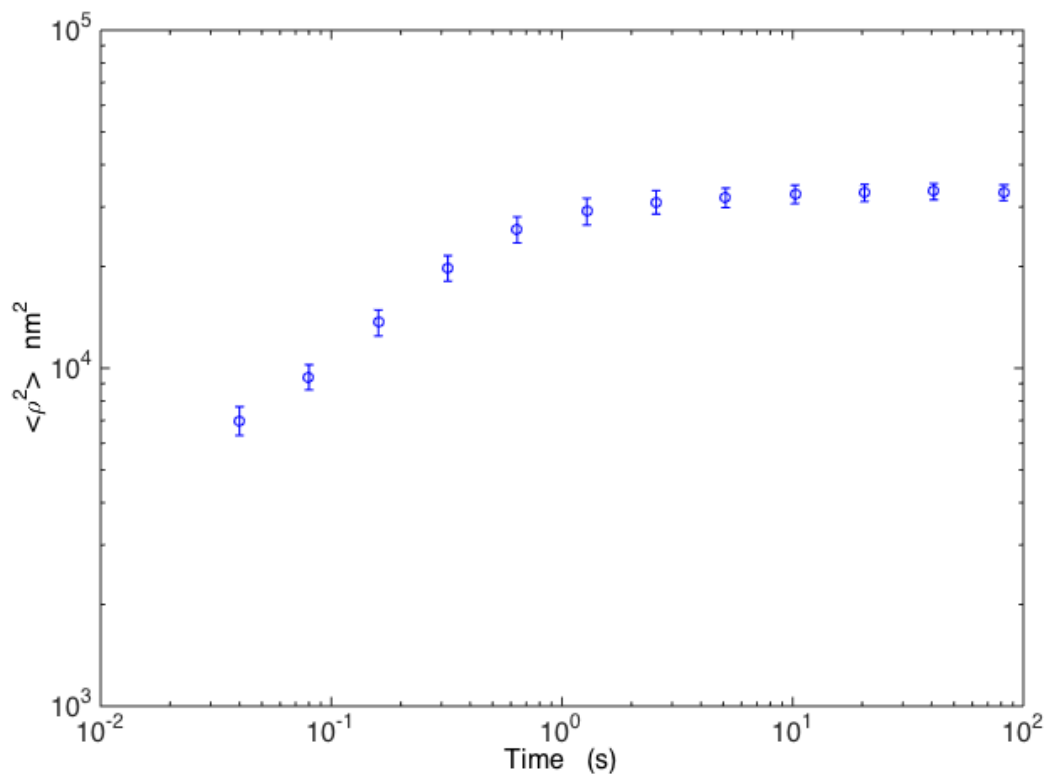


Figure 3-8 Mean square excursion length (ρ square in log axis) vs. time plot in log axis. The mean square excursion, $\langle \rho^2 \rangle$, was calculated with different time intervals. The time required for a representative excursion value depends on the viscosity of the medium and the ionic condition of the buffer as reported by Kumar *et al.* [40]. The plot shows that the excursion value does not change significantly after 4 seconds.

Figure 3-8 shows different time averaged excursion values for 480 nm diameter beads in transcription buffer tethered through DNA to Pol I molecules on the surface. The excursion values do not change significantly after around 4 seconds, which is in accordance with the previous results obtained directly linking the DNA to the flow-chamber surface [7].

3.3.3 Comparison of DIC and Dark Field Microscopy

Dietrich *et al.* 2009 were able to use nanoscopic gold particles and dark field microscopy with a TPM setup [5]. Dark field contrast is high and the components are inexpensive, so we also verified our multiplexed TPM technique in dark field microscopy. These measurements employed a total magnification of 20X, instead of the 40X total magnification used in DIC as shown in **Figure 3-9**.

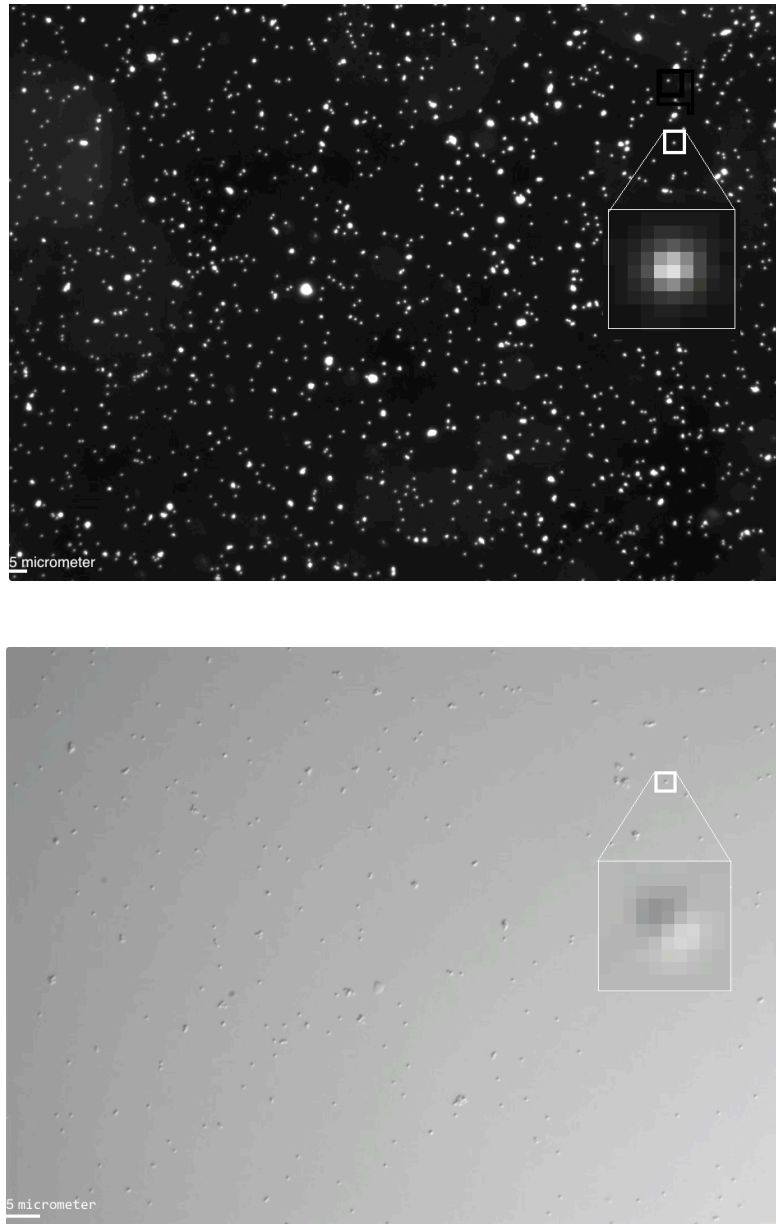


Figure 3-9 Images of representative fields of view in dark field microscopy (top) and DIC microscopy (bottom). The image of a given bead in each image was magnified (inset) to show its pixel composition. The scale bar represents 5 micrometers (lower left corner). Due to the lower magnification (20X *vs.* 40X), the total number of beads was higher in dark field than in DIC images.

The excursion value of the bead was calculated using the Equation 3.2

$$\langle \rho \rangle_{4s} = \left\langle \left(\sqrt{(x - \langle x \rangle_{4s})^2 + (y - \langle y \rangle_{4s})^2} \right) \right\rangle_{4s} \quad \text{Eq. 3. 2}$$

where x and y are the coordinates of the bead at different observation times obtained from the particle tracking routine [40]. $\langle x \rangle_{4s}$ and $\langle y \rangle_{4s}$ are the Cartesian coordinates of the attachment point of the bead resulting from a moving average of 4 seconds. The average excursion values for the DNA tethered by stalled complexes (556 bp) were statistically similar in DIC, and dark field microscopy, as shown by their average values and standard deviations (155 ± 12 nm) and (160 ± 9 nm) respectively (see also **Figure 3-10**). However, the standard deviation of the excursion values measured with the DIC setup was larger than in dark field.

In summary, the comparison of multiplexed TPM measurements with different optical setups confirms that our implementation (see materials and methods) can be successfully utilized with different optical arrangements and different size camera sensors.

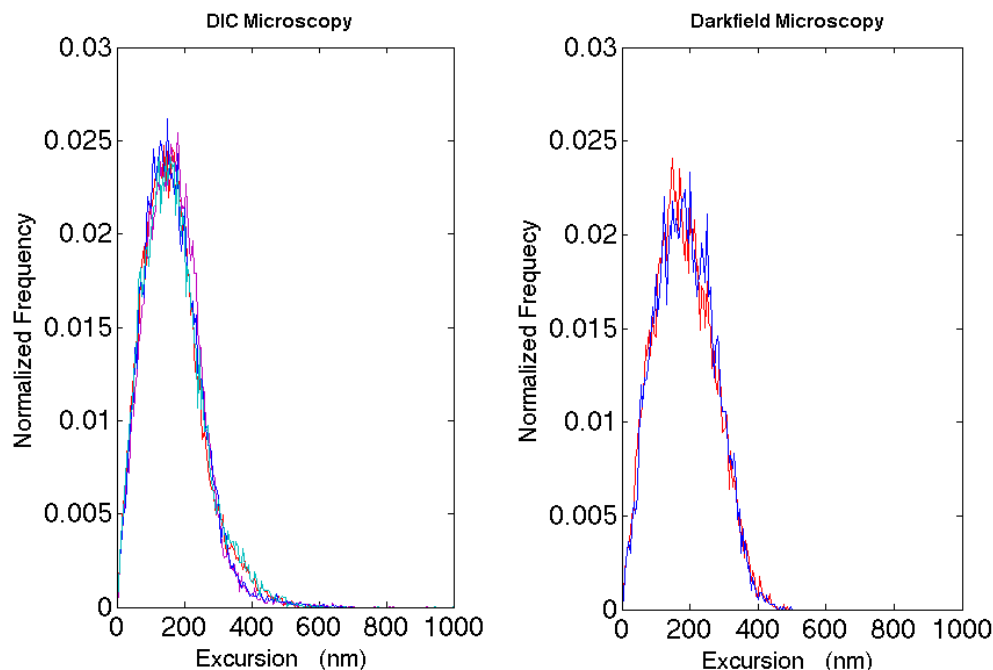


Figure 3-10 Comparison of DIC (left) and dark field (right) microscopy measurements. The distribution of excursion values for a DNA tether 556 bp long is observed to be similar in both cases. The DIC microscopy has a value of 155 ± 12 nm at the maximum probability and dark field had a value of 160 ± 9 nm.

3.3.4 Gyrase Wrapping Experiments

The DNA construct designed to study the wrapping of DNA around gyrase was 335 bp, and wrapping should reduce the tether length by 40 to 100 bp of DNA [58]. Wrapping by gyrase does not require ATP, therefore shortening of the tether due to wrapping is expected to occur after addition of the enzyme to the chamber. However, strand passage does require ATP. Since ATP is not provided in these experiments and wrapping is reversible, the DNA tether length should undergo changes that result in telegraphic-like signals in the traces. **Figure 3-11** shows a representative trace obtained during gyrase wrapping experiments.

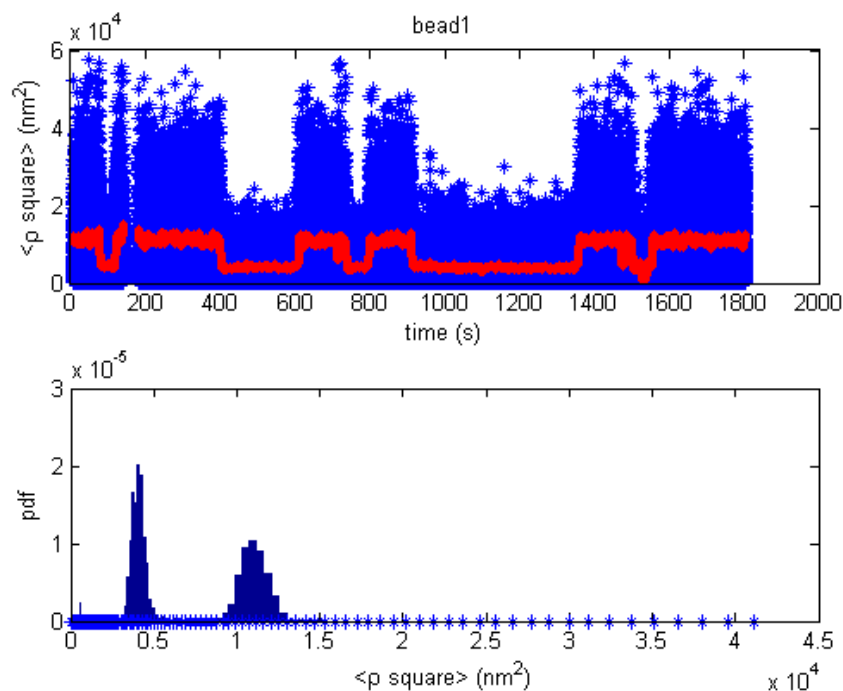


Figure 3-11 A representative trace showing gyrase-induced DNA wrapping and unwrapping (top). Probability distribution of the observed excursion values (bottom). The excursion values obtained during the course of the experiments were plotted as blue points in the top figure. The excursion values were averaged using four second time windows and plotted in red. The two peaks of the distributions in the lower panel indicate the two states of the DNA; unwrapped with the full tether length and wrapped with shortened tether length.

3.3.5 Effects of Compression on the Movie file

Initially all the video was recorded using uncompressed data, since it is best to track particles using uncompressed movie files which contain raw pixel values. However the sizes of these files approaches 35 GB, making compression necessary for both storage and the transfer purposes. A general compression method, such as zip or gzip, for storage after the acquisition of coordinates is not sufficient, since it only allows a compression ratio to 2:1. Also, the time required for compressing and uncompressing averages around 2 hours. The lossless H264 conversion also (FFMPEG,

H264 lossless profile) was able to compress only 2:1 ratio. Hence, a “lossy codec” was used for encoding, which is more time and disk-space efficient. It was found that mp4 file compression with the H264 algorithm gives the best compromise between file size and image quality. By using an open source video encoder (Miro Video Encoder) software and open source H264 codec (FFMPEG, H264 profile), nearly 600:1 compression ratio was achieved with 50 MB of mp4 movie file as output. The implementation of the mp4 movie tracking preserved all the features with the same excursion average value, as shown in **Figure 3-12**. Particle tracking with the mp4 movies required the 2010 or later version of MATLAB and Windows 7 or Mac osX 10.6 operating systems. Although there are some external libraries such as Matlab VideoUtils, which permit the analysis of mp4 files with older versions of Matlab and Windows XP operating system, the implementation of these external libraries was not investigated.

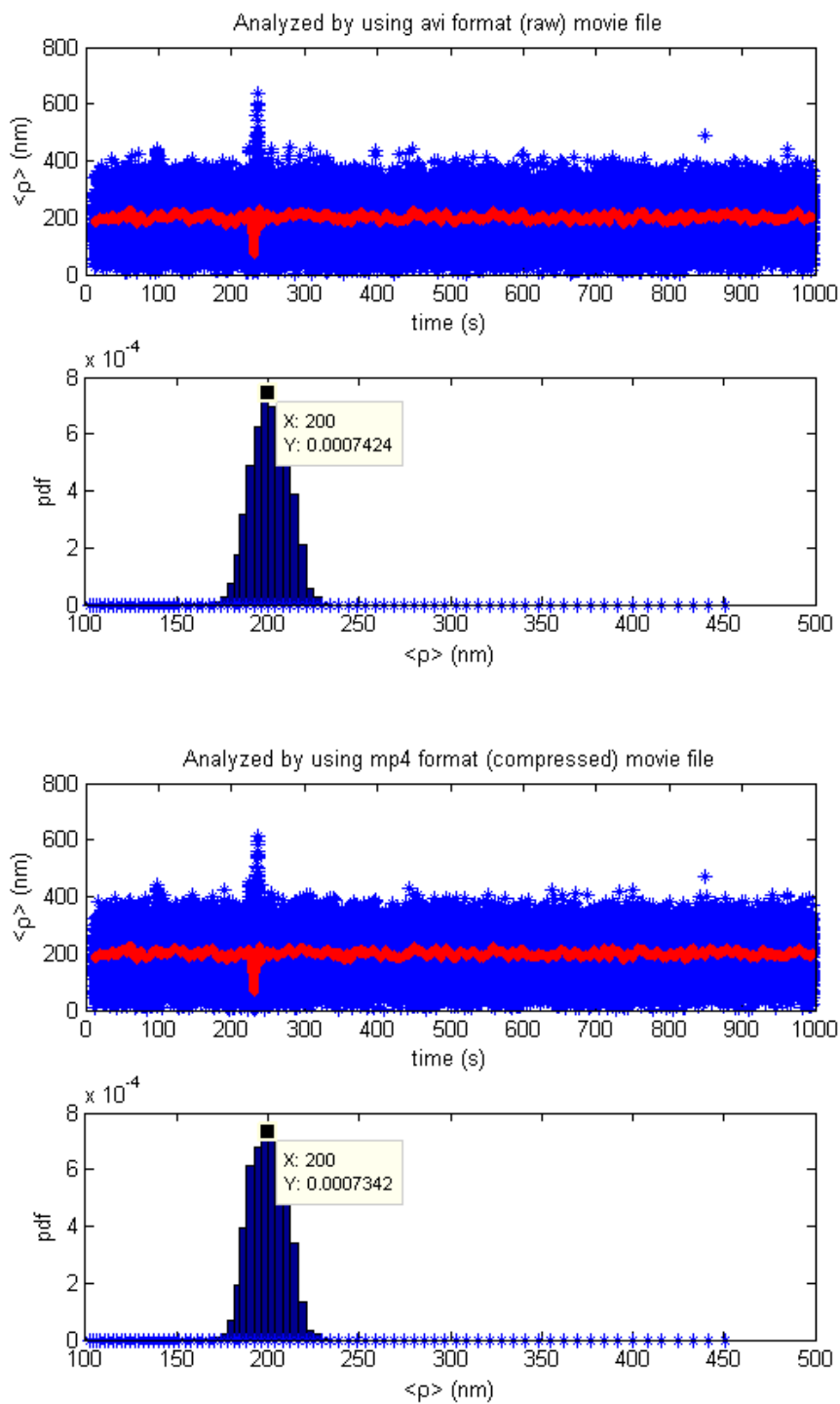


Figure 3-12 The accuracy of the compressed experimental data. The trace of a stalled tether that had a 556 bp DNA length was analyzed using the raw AVI file (upper two figures). The same bead was also analyzed by using the video compressed by FFMPEG H264 codec and Miro Video Converter (bottom two figures). Analysis of the compressed data produced the same excursion value (200 nm) as the uncompressed video file.

3.4 Discussion

Our implementation of the TPM technique permitted observation of transcription events with low restart efficiency. The number of experiments and the efforts to obtain a similar amount of output would have required at least 10 fold more experiments with the conventional TPM approach. Previous attempts to increase TPM throughput relied on a clean-room fabricated chamber and custom software. However, our development on the TPM technique does not involve any special fabrication facility nor does it require any particular software other than Matlab and Labview packages. Our offline analyses also have several advantages. First of all, it is possible to re-analyze the experiment with different tracking algorithms or different parameters and compare the results. It is also possible to make a quality control assessment such as signal-to-noise ratio, or the accuracy of the tracking algorithm. For example, during the course of our research, previously the average of a few moving beads was used to eliminate the drift [4]. Then, it was found that even a single stuck bead was more effective than several moving beads to determine the drift. As a result, the experimental data have been re-analyzed and better drift-free traces were obtained. With the implemented setup, it became possible to bypass the problem of limited computer disk storage.

Chapter 4

Single Molecule Measurements of RNA Polymerase I Elongation

4.1 Background

Almost 40 years after the discovery of the three different types of RNA Polymerases in eukaryotic cells [16], most of the attention has been devoted to Pol II, since it transcribes all of the protein-coding genes and therefore is directly linked to protein synthesis, regulation of transcription and to cell differentiation. However, In 1999 Warner *et al.* discovered that more than 60% of the transcriptional activity of growing cells is due to Pol I [29]. Pol I activity also changes by more than four fold during the cell cycle [59]. The high copy number of rDNA genes in eukaryotic genomes (400 tandem ordered repeats in mammals) also indicates the importance of Pol I transcriptional activity [60].

As the importance of the Pol I has become apparent, researchers have focused on revealing the structure of Pol I in order to highlight differences and similarities with respect to Pol II. Kuhn *et al.* and Cramer *et al.* fitted the Cryo-EM structure of Pol I to the Pol II crystal structure [27, 61]. Their hypothesis was that if the structure was highly conserved in the two polymerases, as predicted by the similarity in their sequences, then Pol I and Pol II might also have the same mechanism of transcription and same kinetic properties. These studies confirmed that both polymerases have a highly conserved active catalytic site. However, it is also known that the rate of elongation rate by Pol II and the duration of its pauses can change drastically depending on the promoter and co-transcriptional factors [62, 63]. Since the rRNA promoter and most of the co-factors for transcription by Pol I are different than the promoters and co-factors recognized by Pol II, the assumption that both Pol I and Pol

It might have mechanistic similarities, simply based on the comparison of their active cores, was not justified. This led to specifically focus on the Pol I transcription.

In 1998, Keener *et al.* successfully reconstituted *in vitro* the basal complex for transcription by Pol I from purified components which included Upstream Activation Factor (UAF), TATA Binding Box (TBP), Core Factor (CF) and rDNA [64]. This success paved the way to study the mechanisms of Pol I transcription. In 2012 Aprikian *et al.* found that a protein called Rrn3p also enhances the processivity of Pol I transcription by increasing the stability of Pol I on the rDNA [53]. The proposed mechanism for basal Pol I transcription is shown in **Figure 4-1**.

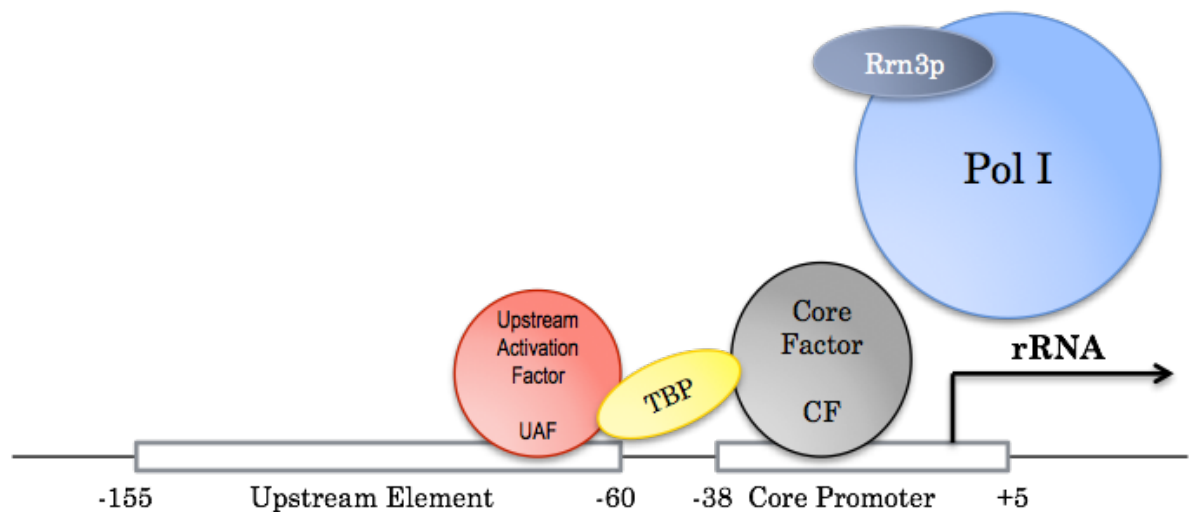


Figure 4-1 Basal requirements for an efficient *in vitro* Pol I transcription. The Upstream Activation Factor (UAF) binds to the upstream element on the rDNA which enhances the initiation of Pol I. The TATA Binding Box protein (TBP) binds to the TATA region before the promoter as for other polymerases. The Core Factor (CF) consists of 5 small proteins, and plays

an important role in the promoter recognition process by Pol I. Rrn3p pre-binds Pol I, and increases the stability of Pol I on the rDNA.

The purpose of my work was to study transcriptional elongation by Pol I at the single molecule level rather than using bulk assays. In order to achieve this goal, first, it was needed to find an efficient protocol to monitor the elongation of Pol I within its functional lifetime of about two hours, at room temperature. Then, the data that showed elongation were collected and analyzed to extract the mechanistic characteristics of elongation by Pol I.

4.2 Materials and Methods

4.2.1 Fabrication of TPM microchambers

The microchambers were prepared fresh before each experiment to eliminate any possible source of contamination. The experimental strategy matched that illustrated in panel B of **Figure 1-1** in chapter 1. Each chamber had a volume of approximately 20 μL . A detail description of the microchamber preparation may be found in Chapter 3. The microchambers were washed with 400 μL nanopure water. Then, the surface was treated with 40 μL of anti-HA antibody (12CA5; stock concentration of 1 mg/ml, Abcam, Cambridge, MA) diluted 1:1000 and was incubated either overnight at 4 °C in the refrigerator or on the bench at room temperature for a minimum 2 hours. Then washed with 400 μL of transcription buffer.

4.2.2 Preparation of Transcription reagents

The DNA template was a segment of the rDNA sequences of *Saccharomyces cerevisiae* (generally referred to as yeast). The segment was inserted in the pNOY745 plasmid containing the 35S promoter for further amplification. All cytosines in the first 56-base pair sequence after the promoter in the template DNA were mutated to guanines, in order to stall the transcription when supplemented with only A, U and G nucleotides and to resume transcription when supplemented with A, U, G, C nucleotides.

Two different elongation experiments were designed: In one elongation is monitored as a shortening of the tether, in the other as a lengthening. Each experiment required a distinct template DNA template. The template used in the first kind of experiment was termed “the downstream DNA” template (**Figure 4-2**).

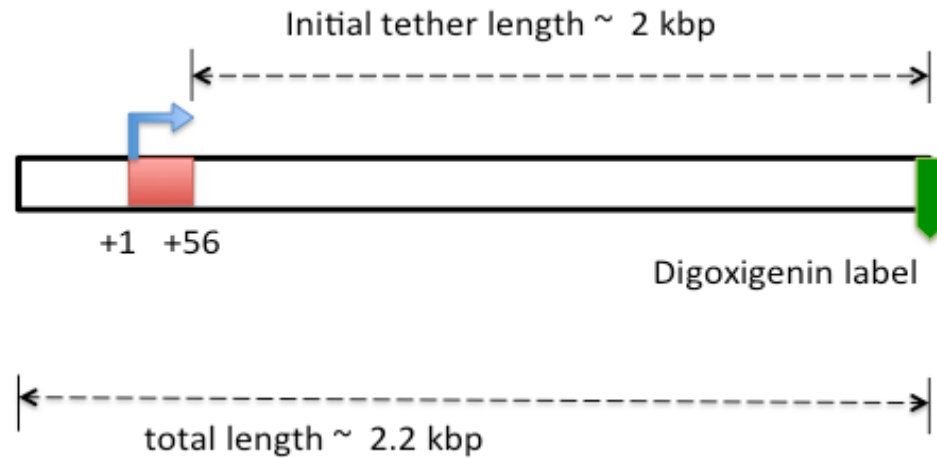


Figure 4-2 Diagram of the downstream DNA template. The first 56 bp sequence along the promoter was modified by mutating cytosines to guanines. Since the anti-dig coated bead is located in the direction of the transcription, downstream of the promoter, the reported tether length should decrease when elongation is restarted.

In the other DNA template, the “upstream DNA”, the location of the bead attachment was reversed (**Figure 4-3**).

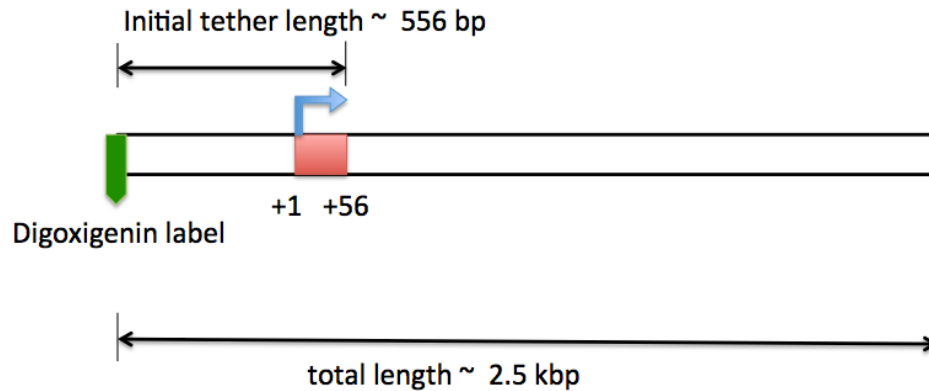


Figure 4-3 Diagram of the upstream DNA template. In this configuration the first 56 bp sequence was mutated as in “downstream DNA”. Since the location of the anti-dig coated bead is opposite the direction of transcription from the promoter, the tether length should increase when the elongation is restarted.

Both the “Upstream” and “Downstream” DNA templates were produced using the Polymerase Chain Reaction (PCR) using labeled and unlabeled primers for the different strands of DNA and high fidelity DNA polymerase. High Fidelity Phusion (New England BioLabs Inc., Ipswich, MA) is relatively slower than the commonly used Taq polymerase but has a proofreading mechanism to ensure the correctness of the sequences. The forward and reverse primers had the following sequence: 5'-ccaaagactttgatttctcgta-3' and digoxigenin-labeled 5'-ccaaagactttgatttctcgta-3', respectively. PCR conditions were identical for both templates, except that the primers for the Downstream DNA had the following sequences: Digoxigenin-labeled 5'-atggtgaaagttcctcaagaat-3' and 5'-cgtttctcagttggtggagtga-3'. The PCR was performed by mixing the following materials in the thin walled thermocycler tube:

- 32.5 μ L H₂O
- 10 μ L 5X Phusion HF buffer
- 2.5 μ L 10 μ M forward primer
- 2.5 μ L 10 μ M reverse primer

- 1 μL (50pg) template DNA
- 1 μL 10 μM dNTP
- 0.5 μL 10X Phusion DNA Polymerase

The thermocycler was programmed to run the NEB2200S program, which consists of the following sequence of temperatures:

1. 95 °C for 3 min, initialization for hot-start polymerase
2. 94 °C for 1 min, denaturation for melting DNA, breaking hydrogen bonds and conversion from double stranded DNA to single stranded DNA
3. 50 °C for 1 min, annealing of primers to the single stranded DNA chains
4. 72 °C for 2 min, elongation of DNA polymerase for adding complementary nucleotides and extending the double stranded DNA
5. Go to 2, 35X, repeat the steps between 2 to 5 to produce more DNA samples
6. 72 °C for 2 min, final elongation for ensuring that all single stranded DNA were extended
7. 55 °C for 1 min, final re-annealing to ensure the correct re-annealing of the single stranded to double stranded DNA
8. 37 °C for 1 min
9. 4 °C forever, for short-term storage

After PCR, the products were purified with a PCR purification kit, (Qiagen; Germantown, MD) and analyzed by gel electrophoresis. Their length was confirmed by comparison with a known, standard DNA ladder. All gel electrophoresis assays were run with a 1% agarose gel in TAE buffer (**Figure 4-4**).

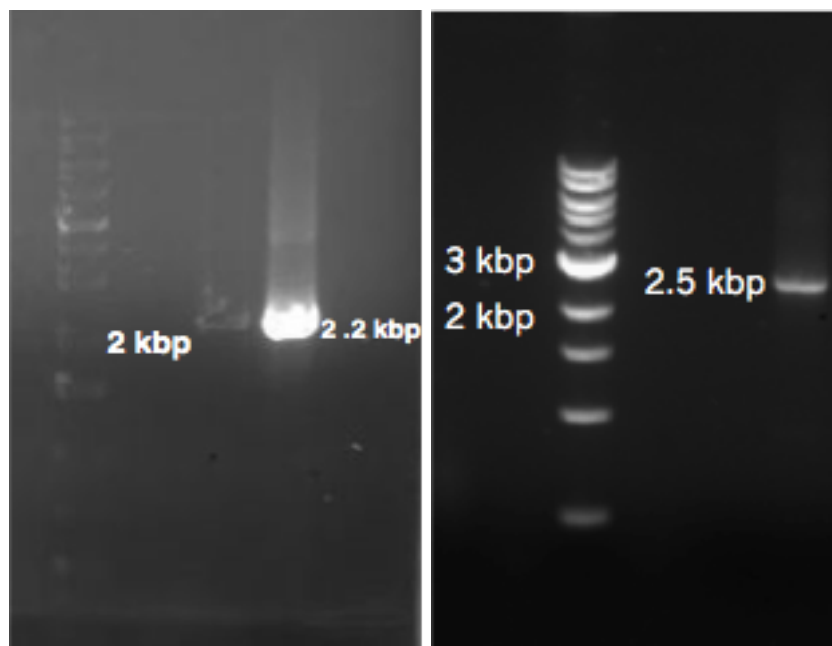


Figure 4-4 Representative gel images of the purified PCR products for the “Downstream” (left panel) and the “Upstream” rDNA (right panel) templates. The DNA ladders appear in the leftmost lane in each panel.

The purification of Pol I, TBP and the CF were described by Schneider *et al.*, 2012 [54]. The stock enzyme was kept at -80 °C in aliquots sufficient for 3 runs of experiments.

The transcription buffer contained 20 mM Tris-acetate, 100 mM potassium

glutamate, 8 mM magnesium acetate, 2 mM dithiothreitol (DTT) and was supplemented with 0.5 mg/ml α -casein. The buffer was prepared at a concentration 2.5 times higher than needed for the experiment and diluted to 1X concentration when required. The pH level of the concentrated buffer was adjusted to pH 7.9 and then filtered with 0.1- μ m syringe filters in order to prevent contamination during preparation steps.

4.2.3 Sample Preparation

The stalled transcription complexes were prepared as follows. First, 43.1 μ l of transcription buffer were mixed with DNA template 0.5 pmol. Then, core factor (CF) TATA binding protein (TBP) for final concentrations of 0.3 pmol, were added to the mixture and incubated for 3 minutes. Then, of Pol I-Rrn3p pre-bound complex for a final concentration of 0.25 pmol were added to the mixture and incubated for 10 minutes in order to facilitate the formation of the closed complex. After 10 minutes, final concentration of 200 μ M ATP, UTP, and GTP mix were added to the mixture and incubated for 3 minutes to form the open complex and initiate transcription which proceeded to elongation for the first 56 base pairs downstream of the promoter and stalled for lack of CTP. All elongation complexes were therefore synchronized. 20 μ L of stalled complexes were added to the microchamber and incubated for the 15 minutes to facilitate the conjugation of the hemagglutinin (HA) tag on the carboxy terminus of the Pol I to the anti-HA molecules nonspecifically adsorbed on the flow-chamber surface. Then, the microchamber was flushed with 400 μ L of transcription

buffer to eliminate unconjugated stalled complexes. Meanwhile, 1 μL of 480-nm-diameter antidigoxigenin-coated polystyrene beads (Indicia Biotechnology, Oullins, France) were diluted in 49 μL of transcription buffer and vortexed for 15 minutes. The beads were then added to the chamber and incubated for 15 to 20 minutes to favor labeling of enzyme tethered DNA. Lastly, the non-conjugated beads were washed out of the microchamber with 400 μL of transcription buffer.

4.2.4 TPM Measurements of stalled and elongating Pol I complexes

First, the Brownian motion of the stalled complexes was recorded for five minutes. This served as control data in order to check the symmetrical motion of the beads and to confirm the tether length. After five minutes, 200 μM A, U, G, C nucleotides in 25 μL transcription buffer were gently added to the chamber. After addition of NTPs without any pausing, data acquisition was continued for ten more minutes.

4.2.5 Simulations

Simulations were performed to test the hypothesis that the experimentally observed pauses were random and not sequence specific. To the best of my knowledge, this simulation is the first study that compares a random walk process and random pauses with the experimentally observed pausing events during elongation steps of polymerase. To simulate the behavior of Pol I, I assumed that its motion along the DNA is a one-dimensional random walk measured in units of base pair per seconds. It was

also assumed that the directed motion and the random motion of Pol I can be separated. At every step, polymerase can move either right (+ direction) or left (- direction). The random +1 or -1 steps were generated with frequency higher (100 times more) than the rate at which the experimental data were generated, 30 frames per second (fps) to better approximate Brownian motion. For example, to simulate two seconds of motion with 30 fps, 6000 steps were generated but every 100th point was treated as an observable. The Equation 4.1 was used to calculate the step size ;

$$D = \frac{L^2}{2\tau} \quad \text{Eq. 4. 1}$$

where τ is the characteristic time per step.

The diffusion coefficient (D) in Equation 4.1 was found by a linear fitting. In order to calculate the diffusion coefficient (D) from the mean square displacement (MSD) *vs* time graph MSD, it was needed to find the coordinate vector corresponding to diffusive motion. The coordinate vector was generated by subtracting the directed motion coordinates which were found from the mean velocity multiplied with the time points from experimental positions. Each random +1 and -1 was multiplied by the step size, L. Then, the random motion of the polymerase was found by integration of the steps from zero to t' . Therefore, the random positions can be found using the Equation 4.2:

$$x_{random} = \sum_{x=0}^n random(nL) \quad \text{Eq. 4. 2}$$

After obtaining the random motion of the polymerase, the directed motion of the system was obtained by multiplying the average velocity by the time. As a result, the trajectories for the polymerase motion on the DNA was calculated using Equation 4.3:

$$\mathbf{x}_{trajectories} = \mathbf{x}_{directed} + \mathbf{x}_{random} \quad \text{Eq. 4.3}$$

In order to simulate the system more realistically, the diffusion and the average velocity values were calculated for each individual polymerase-DNA complex, then inserted as parameters into simulations.

4.3 Results and Discussion

Figure 4-5 shows the schematic setup and an elongation trace from the “Upstream DNA” template. The trace in **Figure 4-5** starts above 500 bp since it corresponds to the TPM signal expected for a transcription complex stalled at position +56 (see Materials and methods). These control data were captured for 5 minutes to check the initial tether length (see trace in **Figure 4-5** between 0 to 300 seconds). Image acquisition continued after addition of 200 μM of all four nucleoside triphosphates (NTPs). This substrate concentration has been the standard condition in several previous *in vitro*, bulk studies Pol I activity, and is thought to be saturating for transcription elongation rate. The image was blurred for about 1 minute due to buffer flow. Restart of transcription elongation resulted in an increase in DNA tether length as shown in **Figure 4-5**.

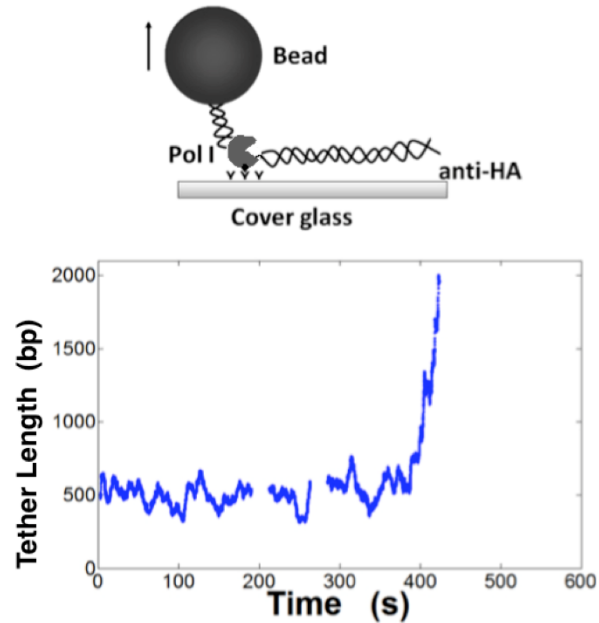


Figure 4-5 Schematic of experimental setups (Top) and representative elongation trace for the “upstream DNA” template (Bottom). A 480 nm anti-dig labelled bead was attached to the upstream end of the DNA template. The hemagglutinin (HA)-labelled Pol I of a stalled complex attaches to the anti-HA coated cover glass. After addition of NTPs, elongation restarts, and hence tethered DNA length increases. Data were culled (blank segments of trace) when sticking of beads to surface occurred.

Figure 4-6 shows the experimental setup and a representative trace of a “Downstream DNA” tether. (see Materials and Methods). Together, these data strongly support the idea that the changes in tether length observed in these experiments are due to transcription elongation by Pol I on single rDNA segments. Although both experimental designs were effective, the setup described in **Figure 4-5** was chosen for all subsequent analyses.

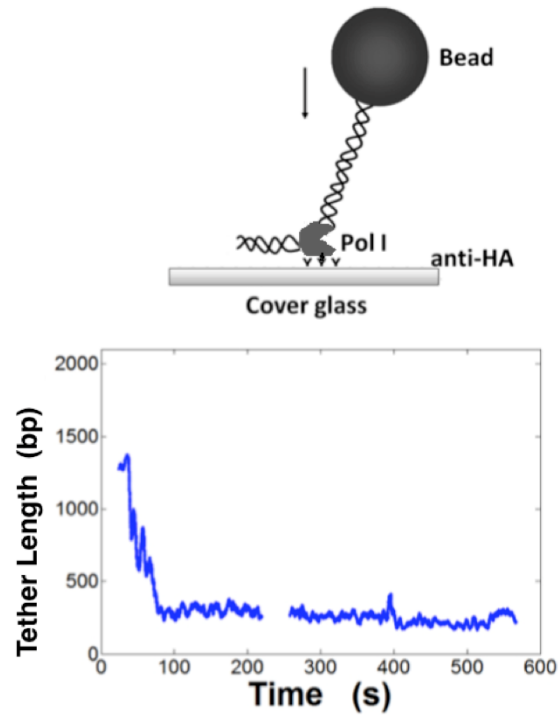


Figure 4-6 Schematic of experimental setup (Top) and representative elongation trace (Bottom) for the “Downstream DNA” template.

4.3.1 Elongation Rate

To quantify transcription elongation rates of individual polymerases, the TPM excursion values were monitored and a moving average of 10 data points was applied to establish the position of Pol I along the template during elongation. Then the differences between successive mean values were divided by the time interval between them (0.33 seconds), to determine the rates of polymerization. **Figure 4-7** shows the frequency distribution of all the rate values obtained in this way.

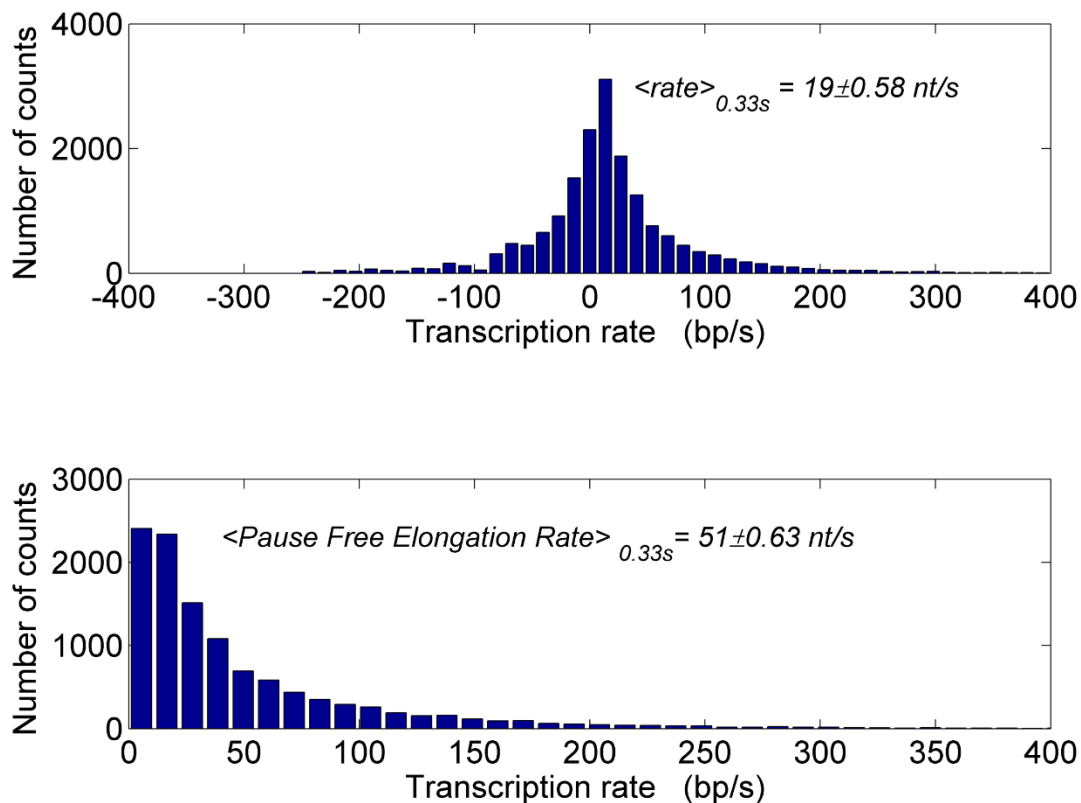


Figure 4-7 Pol I elongation rates. The average rate (upper panel) includes pausing and backtracking events. The rates were calculated by using a moving average of ten data points, or 0.33s, and the reported errors are SEMs. The pause free rate (lower panel) was found by considering only forward elongation rates. For this purpose, the rate values were eliminated that were equal to, or smaller than, zero, calculated using the difference between data points corresponding to video frames separated by 10 time intervals. Then, the mean of the remaining positive rate values were calculated to obtain an average pause-free rate.

The average elongation rate was found to be $19 \pm 0.58 \text{ nt/s}$ in the presence of 200 μM NTPs. This finding is consistent with the rate of $\sim 20 \text{ nt/s}$ measured using *in vitro* bulk assays [54]. On the other hand, ignoring pauses or potential backtracking, by eliminating the rate values which were equal to, or smaller than zero, and considering only forward elongation events, the pause-free elongation rate was found to be $51 \pm 0.63 \text{ nt/s}$ (**Figure 4-7**), close to the rate of 60 nt/s estimated for *in vivo* transcription based

on electron microscopy studies [35].

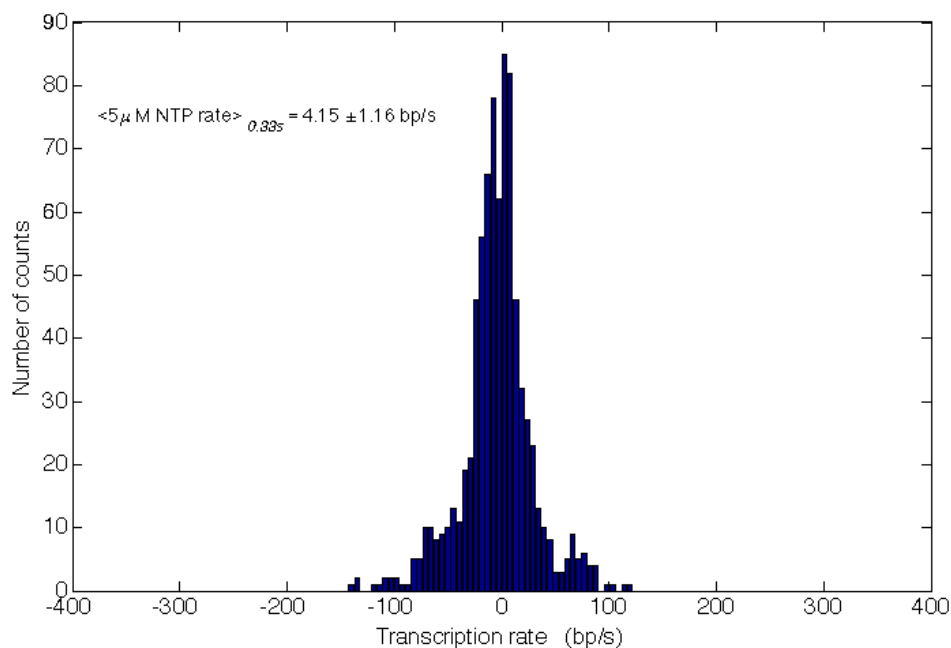


Figure 4-8 Distribution of rates in the presence of 5 μM NTPs. The average rate was 4.15 ± 1.16 nt/s (SEM).

When the concentration of NTPs was decreased to 5 μM , the average elongation rate decreased to 4 nt/s (**Figure 4-8**), as expected based on previous studies using sub-saturating NTP concentrations [54]. All subsequent analyses were performed in the presence of 200 μM NTPs. Control measurements in the absence of NTPs yielded no net change in tether length over time (zero elongation rate) (**Figure 4-9**).

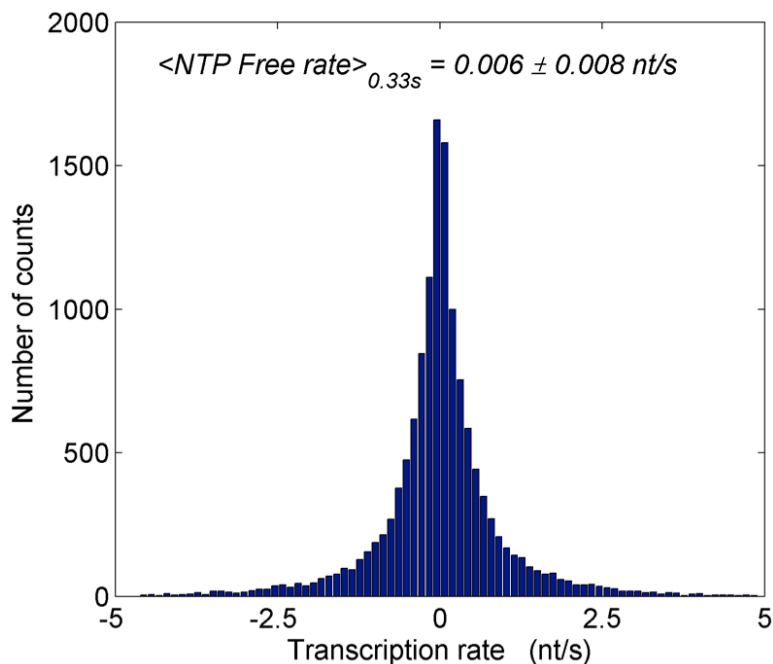


Figure 4-9 Frequency distribution of the elongation rates calculated for control experiments before addition of NTPs. The error represents the standard error of the mean (SEM).

4.3.2 Processivity RNA Polymerase I

One clear, but somewhat surprising observation evident in the raw TPM data was that the majority polymerases did not reach the end of the 2kb template. In fact, only 1 out of 42 elongation complexes reached the end (followed by release of the bead).

Figure 4-10 shows the locations at which transcription arrests were observed in each of the 42 templates observed. The templates, numbered chronologically, were ordered according to their arrest length. In order to distinguish between paused complexes that might resume elongation and terminally arrested complexes, data were recorded for at least 15 - 25 minutes, approximately ten fold longer than the time expected to be required for transcription of a 2 kbp template, based on published *in vitro* Pol I

transcription data [31]. Processivity of a polymerase describes the ability of the enzyme to transcribe to the end of the template. Our TPM data demonstrate that Pol I is not highly processive *in vitro*. This finding contrasts with a number of observations *in vivo* (e.g.[62]).

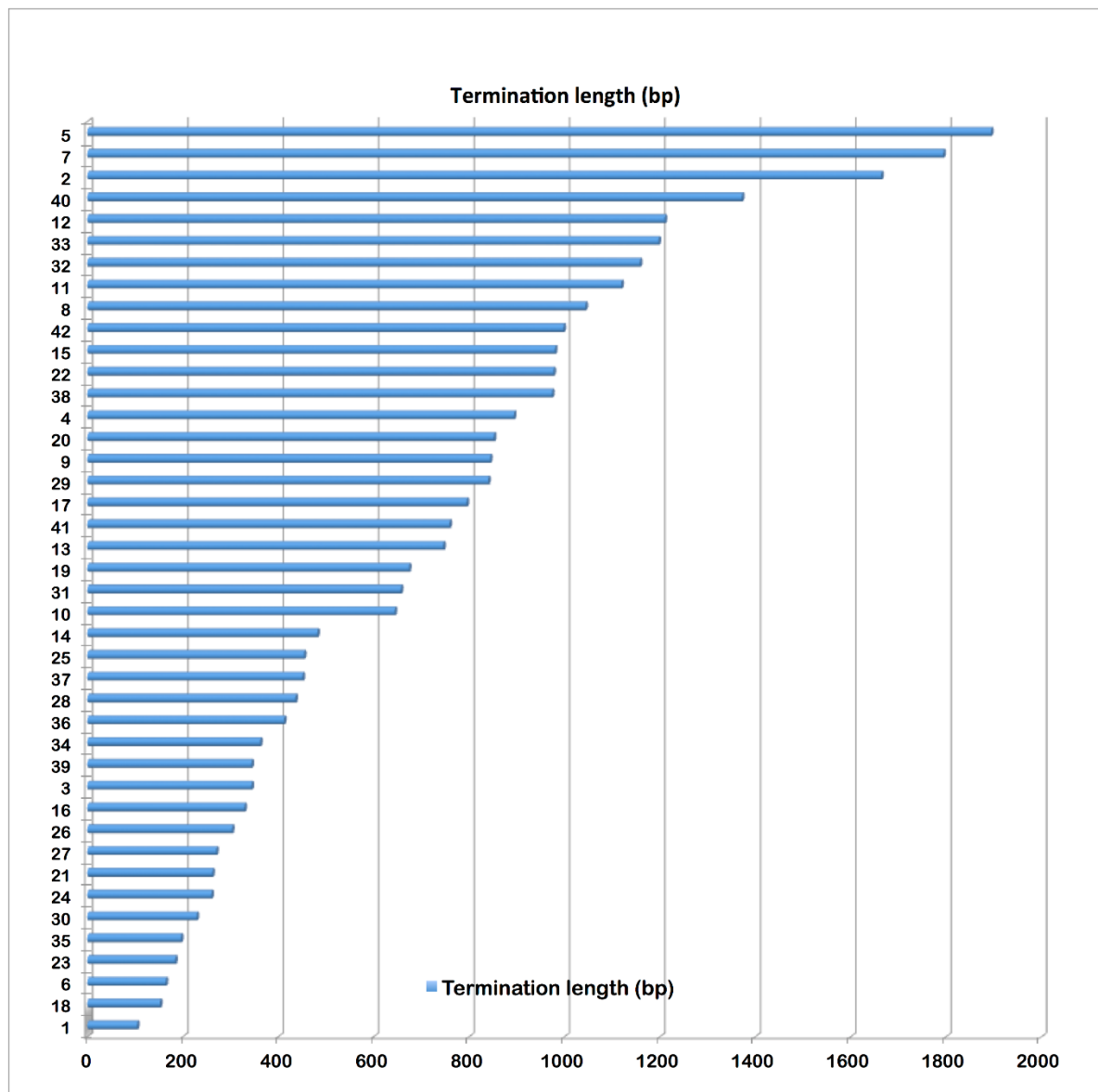
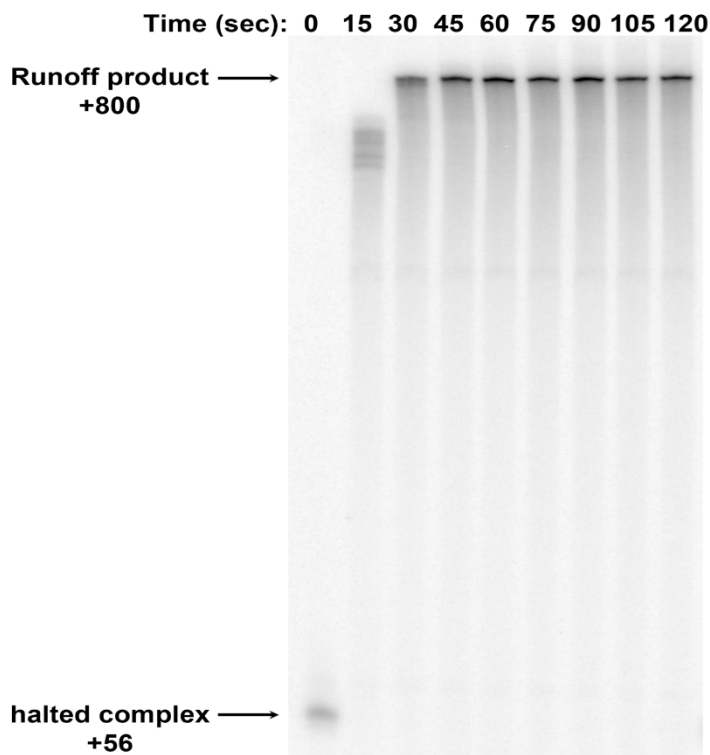


Figure 4-10 Pol I processivity measured by TPM. Most complexes terminated elongation at different DNA locations, with only one complex out of forty-two reaching the expected run-off site.

In order to determine whether this defect in processivity was an artifact of our single-molecule analysis or a general feature of Pol I transcription *in vitro*, Our collaborators, Dr. David Schneider and Krysta Engel from University of Alabama Birmingham performed bulk biochemical assays of Pol I transcription (as described previously in [31]). In this experiment, the halted complexes at +56 and the 800-base runoff product were clearly observed (**Figure 4-11**). To measure the fraction of Pol I complexes that reached the end of the template, α -³²P GTP was included in these reactions, the band intensities at +56 and +800 were normalized for the number of G residues in the respective products. The normalized values for +800 were then divided by the values for +56. This value reports the fraction of halted complexes that result in full-length product. The average for three independent series of transcription reactions indicated that only 31% of complexes yield full-length product. This value is close to, but lower than the processivity observed in single molecule assays where 55% (23/42) complexes reach ~800 base template length; **Figure 4-11**).



Percentage of halted complexes that runoff = 31.3 +/- 0.7

Figure 4-11 Pol I processivity measured in bulk. Transcription was initiated from a template similar to that described for the TPM measurements described above (**Figures 4.5-4.10**) except that in this case, there was no dig-label and the downstream end point was +800 with respect to the transcription start site. Transcription was initiated in the presence of core factor, TBP, Rrn3 and Pol I, using 200 μ M ATP, UTP and 20 μ M GTP plus α 32P-GTP. Transcription elongation complexes halted at +56, a sample was collected in phenol, and CTP was added to 200 μ M final concentration. Samples were collected into phenol as a function of time, precipitated, resuspended in formamide loading dye and analyzed by denaturing gel electrophoresis and phosphor-imaging. This experiment was repeated three times and averaged data are shown with error = 1 standard deviation

Together these data demonstrate that under these conditions *in vitro*, Pol I is not as processive as *in vivo*. Thus, it is likely that additional factors contribute to processivity

of Pol I *in vivo*, and these factors or conditions remain to be discovered.

4.3.3 Pause sites on rDNA

In the single molecule assays, transcription elongation stopped at different sites on each DNA tether analyzed. **Figure 4-12** shows the distribution of the observed pause sites for all the traces.

Since not all DNA tethers were transcribed to the end, the data were weighted by the number of complexes that reached any given length in order to directly compare pause frequency at each position of the template (raw numbers are presented in **Figure 4-13**). These sites were interpreted as locations that predispose the enzyme to pause. The most frequent pausing was observed ~100 bp downstream of the stall site, and pausing was more probable in the first 300 bp than in the rest of the template.

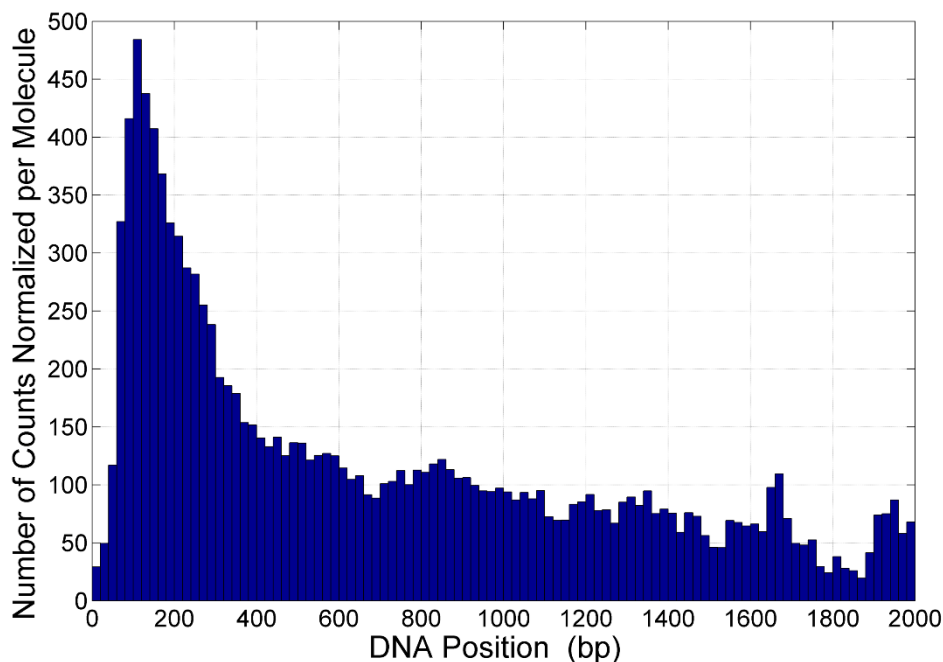


Figure 4-12 Histogram (bin size is 20 bp) of lengths of DNA tethers observed during transcription by Pol I. The data at each length is normalized by the number of tethers with active transcription during observations at that length in order to uniformly emphasize pauses across the entire template (see Results). In other words, since most molecules did not exhibit run-off transcription, the population of pausing events was higher at the beginning as opposed to the end of the template, because there were more tethers that exhibited active transcription at the beginning of the template. For this reason, the number of pausing events was normalized in a piece-wise fashion to give a balanced display. The number of observations of a given length was divided by the number of tethers that reached or exceeded that length. For example, transcription progressed along all of the 42 tethers through the first 100 bp, therefore counts in that interval were divided by 42. For the longer tethers the data was collected from, and normalized for progressively fewer tethers, and finally the counts between 1900 bp to 2000 bp were divided by one, since only one tether was transcribed completely.

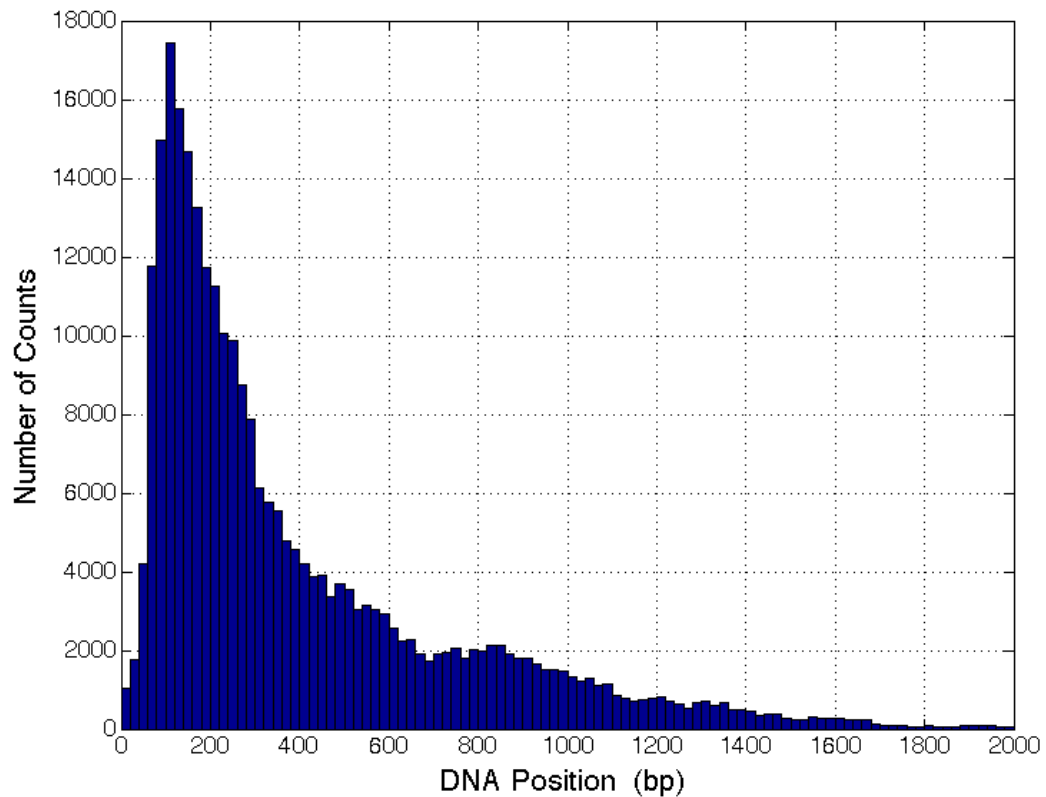


Figure 4-13 Distribution of pause locations during elongation (raw data). Bin size = 20 bp. This histogram was not weighted for the different tether lengths at which transcription arrested. Therefore the population of pausing events should be higher in the first 100 bp than between the 1900th and the 2000th base pair because there are more events for the first 100 bp.

Interestingly, the Weissman laboratory has recently identified a sequence element that favors pausing by bacterial RNA polymerases *in vivo* [65]. Sequence analysis of the rDNA in the vicinity of the predicted pause event identified the following sequence beginning at position +163: **GGgttgaTGCG**. This sequence is very close to the consensus identified by Larson and colleagues [65], differing only in the spacing between the two conserved elements (shown in capital, bold). We speculate that pausing may have functional relevance *in vivo*. Pausing by Pol I could influence

processing of the pre-rRNA [30], thus future studies will focus on detailed characterization of this and other potential sites of transcriptional pausing.

4.3.4 Random Walk Hypothesis

The pausing observed in the Pol I elongation traces could be random or be induced by specific sequences. Most of the RNAP and Pol II studies addressed this issue by modifying the DNA sequence on pause locations and checking for changes in pausing [16]. Pol I only transcribes the ribosomal RNA and in this case, altering the wild type sequences may also affect the mechanism of the enzyme [17]. Thus, my data was simulated using a random walk. The large differences between experimental data and simulations would indicate non-random pausing. **Figure 4-14** shows the frequency distributions of the pause locations along the DNA template as obtained experimentally and via simulation. Since processivity was found to be low, pause events are bound to be lower as one progresses away from the promoter along the DNA template. However, the number of pause events around 200 bp in the experimental histogram indicates that pausing in this region is clearly not random even weighting for the higher probability due to the relative vicinity to the promoter. Remarkable is also the fact that experimental pauses observed at around the 750 bp location occur less frequently than what predicted if pausing was a random, sequence-independent effect. Unfortunately, there were only three transcriptional runs longer than 1500 bp. The lack of high number of events prevents us from commenting about pausing on the further part of the template. The histogram of $x_{trajectories}$ in Eq. 4.3 obtained by simulations were plotted

and compared with the experimental histogram as shown in **Figure 4-14**. The comparison demonstrated that for the first 400 bp DNA, the experimental traces reveal more pauses than predicted if the phenomenon was random. This may indicate that this sequence contains preferred locations for pausing. Instead, it appears that the region around 700 bp, favors elongation versus pausing. The physiological meaning of such sequence-dependent effects on Pol I elongation are still under investigations.

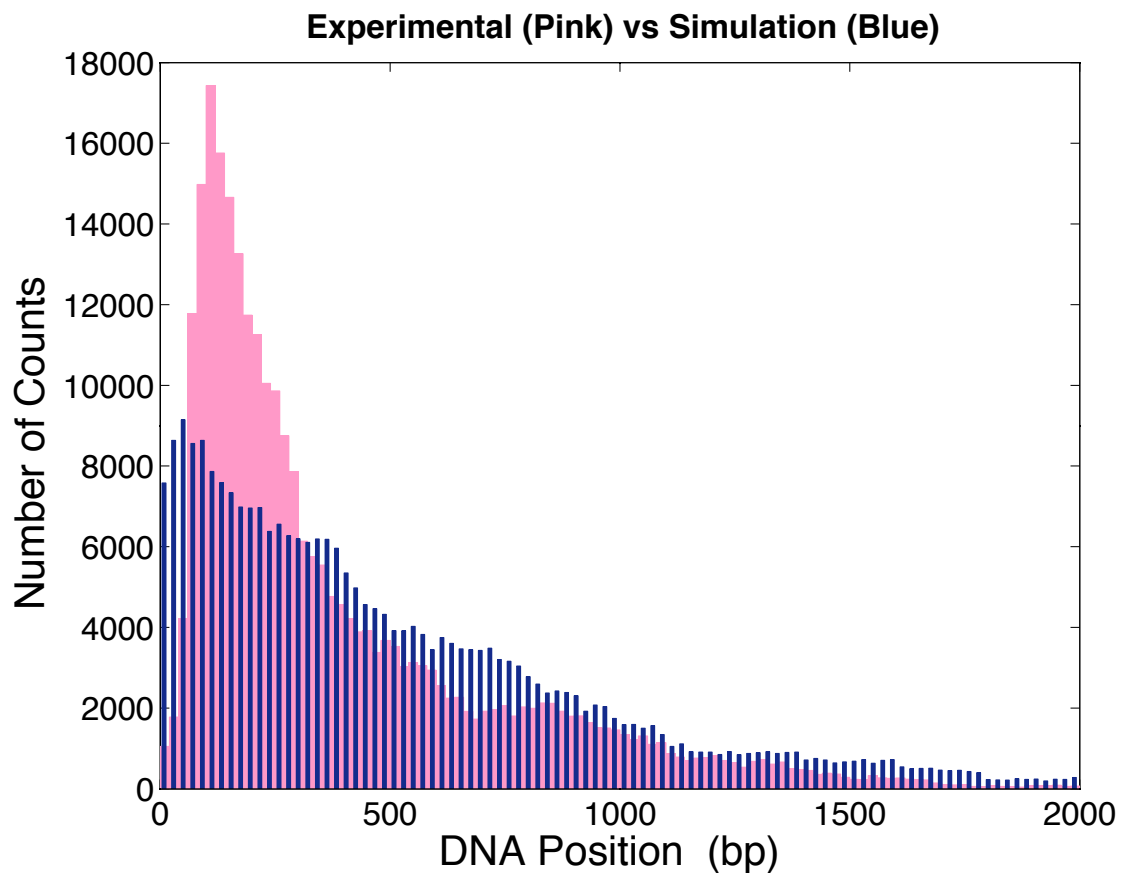


Figure 4-14 Comparison of the pause locations obtained from experiments (pink) and from biased random walk simulations (blue).

4.3.5 Energy Barriers of Elongation

In order to move along the DNA and shift the location of the transcription bubble, Pol I must melt the DNA by breaking the hydrogen bonds between the two strands of the double helical template. There is also another energy barrier to DNA melting due to the favorable base pair stacking interactions between adjacent base pairs along the double helical vertical axis. The free energies for base pair stacking and hydrogen bonding depend on the DNA sequence. Previous studies showed that a decrease in the elongation rate may correspond to an increase in transient pauses [66, 67]. Therefore, it was hypothesized that the energy barrier for melting DNA may facilitate pausing events. In order to test this hypothesis, the free energy for DNA melting was calculated by summing base pair stacking energy and the hydrogen bonding energy. The hydrogen bonding energy was calculated by multiplying 0.25 kcal/mol by two for every A-T pairs and by three for every C-G pairs [68]. Base pair stacking energy for each neighboring base combination was calculated using the table in Bommarito *et al.* 2000 [69].

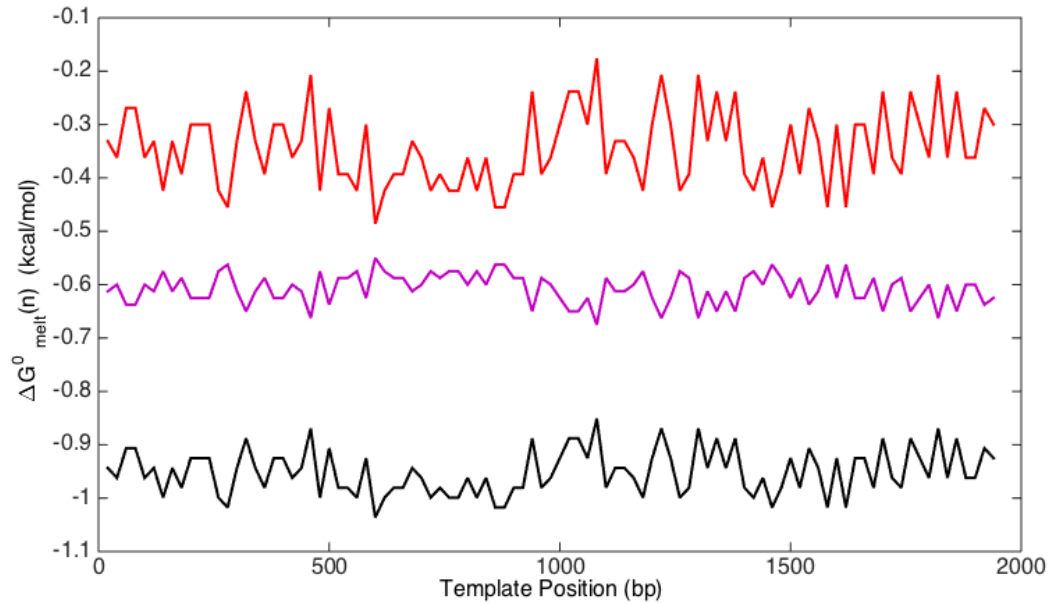


Figure 4-15 Free energy $\Delta G_{melt}^0(bp)$ for the rDNA template (bottom, black) was found by adding base pair stacking energy (top, red) to the hydrogen bonding energy (center, purple). All curves are averaged for 20 bp.

The result of my calculation is shown in **Figure 4-15** and indicates no correlation between pause locations and energy barriers. The free energy required to melt the DNA fluctuated between 0.9 kcal/mol to 1 kcal/mol. Especially for the most prominent pause location observed in the experiments, around 200 bp, there was no significant energy barrier compared to the rest of the sequence.

4.3.6 Kinetic rate of transcription

A series of kinetic simulations and calculations were made to extract kinetic information about elongating Pol I complexes. It was assumed that several species are

involved, including open, elongation, pausing, and backtracking complexes as shown in Figure 3.10. This kinetic model is not formulated in terms of concentrations of the species, instead the probability density of the lifetimes (or wait times as in Xie 2001 [70]) for each species is used.

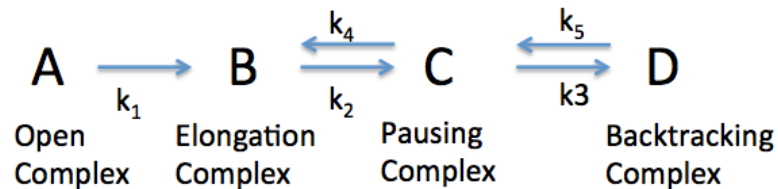


Figure 4-16 The kinetic diagram for the transcription by Pol I which consists of the conversion from open complex to elongation complex with the kinetic rate, k_1 . Then chains of reversible reactions occur from elongation to pausing and then to backtracking complexes.

The following differential equations (Equation 4.4-4.7) were solved with the symbolic toolbox of Matlab.

$$\frac{dP_A(t)}{dt} = -k_1 P_A(t)$$

$$\frac{dP_B(t)}{dt} = k_1 P_A(t) + k_4 P_C(t) - k_2 P_B(t)$$

$$\frac{dP_C(t)}{dt} = k_2 P_B(t) + k_5 P_D(t) - k_4 P_C(t) - k_3 P_C(t)$$

$$\frac{dP_D(t)}{dt} = k_3 P_C(t) - k_5 P_D(t)$$

Eq. 4. 4-7

Then, a simulation was designed to quantify the change of probability in time as shown in **Figure 4-17**. The open complex was chosen as a starting point, which then

moves into the elongation complex, and from here, into pausing and backtracking events with certain probabilities. The first order rates were randomly assigned to verify the model. In experiments, the average elongation rate was measured to be approximately 20 nt/s as explained in Chapter 4. In the simulations, k_1 rate was used (0.1 s^{-1}) which has the same order of magnitude. k_2 , k_3 , k_4 and k_5 were also assigned as 0.005 s^{-1} , 0.02 s^{-1} , 0.03 s^{-1} , 0.02 s^{-1} . The assigned rates for k_2 , k_3 , k_4 and k_5 is at least two order of magnitude smaller than the elongation rate, because in experiments the observed lifetime for pausing events did not exceed about 10% of the total observed events.

At the end of the model verification, mostly the formation of the elongation complex was observed, with a smaller probability of pausing and backtracking, as expected.

It needs to be emphasized that, these values were just used to test the kinetic model, and they needed to be compared more precisely with the experimental data.

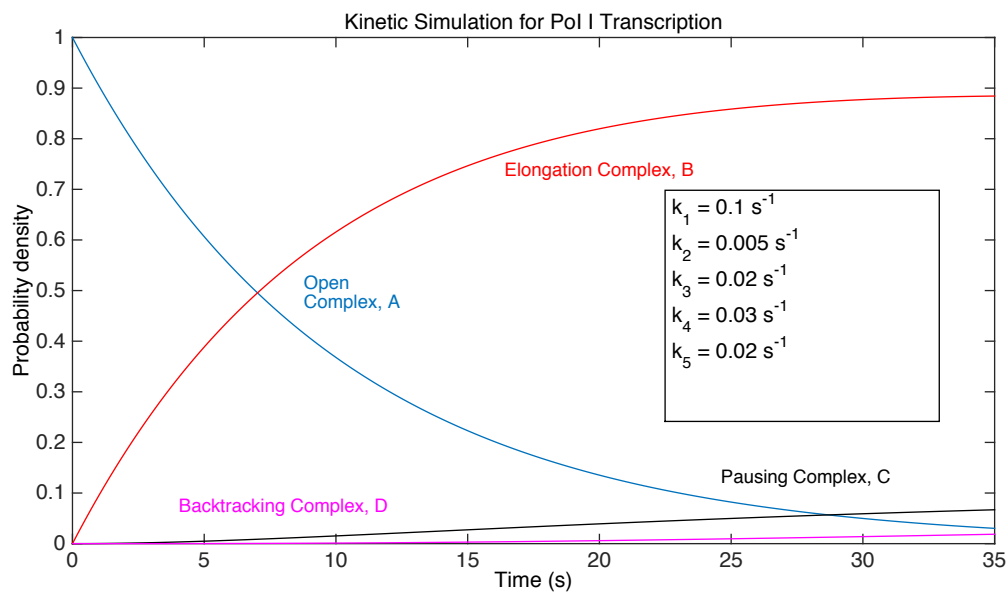


Figure 4-17 The simulation for a kinetic model of 4.16. The open complex (blue line) was converted to elongation complex (red line) and then pausing complex (black line) and backtracking complex (pink line). Since the experimental instances of pausing and backtracking were rare compared to the elongation complex, the rate constants for these events were chosen to be smaller than the elongation rate constant, k_1 , approximated with 0.1 s^{-1} for an elongation rate of 20 nt/s.

Chapter 5

Conclusions

5.1 Prerequisite Experiments: Calibration of TPM Data

Performing TPM microscopy is far simpler than using most other single molecule techniques, such as single molecule Florescence Resonance Energy Transfer (FRET), since TPM does not require a complicated optical setup or the excitation of the dye molecules. However, just like for any other type of assay, conditions must be optimized for every given system of study. In TPM, beads tethered to the surface by multiple DNA molecules, the low number of tethered beads, or the abundance of beads nonspecifically attached to the chamber surface are the most common experimental problems that may reduce the efficiency of TPM experiments. For each new experimental condition, optimal conditions need to be found that minimize these issues. In addition, in order to quantitatively interpret the results of TPM measurements, a calibration curve must be obtained using DNA tethers of known length and in the same experimental conditions. Even though Monte Carlo simulations were implemented to explore the effect of a variety of parameters on the observable bead excursion, among which were DNA tether length, bead size, excluded volume. The results cannot reliably predict experimental findings [36]. Therefore, an empirical calibration curve was built using six different DNA tether lengths (see **Table 2.2**, **Figures 2.4-5**) in the buffer used for the transcription assays. Although the precision of the TPM decreases with the increase of the tether length as shown in the **Figures 2.4 and 2.5**, the calibration curve obtained by plotting the mean square excursion gives a directly proportional relationship between the excursion values and the DNA tether lengths as depicted in **Figure 2-4**. The rigorous selection process of the tethered beads to

be analyzed by assessing the symmetry of radial histograms (**Figure 2-2**) and hierarchically clustering the excursion values (**Figure 2-3**) also facilitated accurate calibration.

5.2 A Must for Low Yield of Transcriptional events: Multiplexed TPM

The data output of single molecule experiments is inherently low compared to that of ensemble studies. Acquiring sufficient data for a meaningful statistical analysis requires tedious repetition of the experiments. This is a common hurdle in single molecule investigations, and it is especially taxing in the case of “one shot” measurements, like most transcription assays. Therefore, some effort has been recently devoted to finding ways to increase the throughput of single molecule assays [71]. However, none of the solutions that have been proposed thus far are easy to implement. For this reason, the Multiplexed TPM setup was developed and the approach that Parthasarati *et al.* established has been altered specifically for tracking the DIC microscopy images as explained in section 3.3.1. Multiplexed TPM was successfully implemented using both DIC microscopy and darkfield microscopy as shown in **Figure 3-9**. However, optical alignment in darkfield microscopy was more time consuming than in DIC. Thus, considering the limited life time of Pol I activity, the latter optical arrangement was used. Multiplexed TPM was not only used to study Pol I transcriptional elongation activity but also DNA gyrase wrapping activity (**Figure 3-11**). Even though, sufficient data were not collected (6 wrapping events) to draw a definitive conclusion about the mechanism of gyrase, these experiments were used to

assess the activity level of *Escherichia coli* gyrase, which indicated what concentration to use in further experiments run by Dr. Fernandez (manuscript submitted).

The significance of the technical efforts described above stems from the fact that TPM has several advantages over other techniques. The characteristic feature of TPM, compared to the other single molecule assays, is the absence of an external force during the measurements. Thus, the system of study is minimally perturbed during observation. This is particularly relevant when studying transcription. For example, it has been shown by Neuman *et al.* that Pol II pauses more frequently as the force applied to the DNA template is increased [66]. The absence of external perturbations, which need to be maintained uniform across the field of observation, makes TPM more suitable for multiplexing [72].

5.3 Pol I processivity

Processivity measures the efficiency with which RNA polymerases reach the end of their transcription template [62]. It should be noted that processivity is different from the rate of initiation, which measures the efficiency with which RNA polymerases start transcription. In yeast, Pol I transcribes one of the longest genes encoded in the genome (~6.7 kb) and previous visualization of Pol I transcription by electron microscopy has shown that Pol I is highly processive [35, 62]. However, both the TPM data reported here (**Figure 4-10**) and the bulk transcription data by Dr. Schneider's group (unpublished data) (**Figure 4-11**) show that Pol I is poorly processive *in vitro* on a

naked DNA template. The length of the DNA template was 800 bp in bulk measurements. In order to compare the processivity measurements of the single molecule assays with the bulk assays, the elongation events that reached to 800 bp location of DNA template were counted and divided by the total number of observations as explained in the section 4.3.2. The single molecule processivity was found nearly 55%. However, only 30% of the complexes reached the 800 bp run-off site in the bulk measurements. Therefore, the single molecule processivity was not lower than bulk assays. Combined *in vitro* data may indicate that one or several factors that contribute to the exceptional processivity of Pol I *in vivo* are absent in the purified system. A small number of transcription elongation factors that influence the Pol I transcription have been described [62, 73-76]. Perhaps one of these factors can directly influence processivity of the enzyme. Alternatively, it is possible that the nascent rRNA which in our assay is not processed by ribosomes may interact with Pol I and interfere with elongation such as R-loop formation reported by El Hage *et al.* [77]. It is also possible that the conditions of the single-molecule and bulk transcription assays contribute to the poor processivity. In any case, these data demonstrate that Pol I processivity is suboptimal *in vitro*, and that TPM can be used to directly address the features that may affect the enzyme's processivity. Since transcription of ribosomal DNA is gaining interest as a potential chemotherapeutic target [33, 34], identification of the factors that directly affect Pol I activity will have an obvious significance for drug discovery.

Theoretically, the frequent arrests in the TPM measurements could be induced by

the tension occurred from pulling the tethered particle that opposes transcription (**Figure 4-6**) [11]. Though being possible, this interpretation is unlikely, because the experimental system was also implemented shown in **Figure 4-5** in which Pol I pulls on an unlabeled DNA template with consequent lengthening of the tether and run off transcription. Neither experimental setup resulted in efficient elongation to the end of the DNA. Furthermore, the bulk assays shown in **Figure 4-11** employ linear, unlabeled DNA templates. Since Pol I was not fully processive in those assays either, it is unlikely that the tagged particle induced any artificial polymerase arrest.

The activity of Pol I is regulated up to four folds during the cell cycle, but in all, Pol I accomplishes more than 60% of the all transcription in the cell. It has been reported that the short-term regulations of Pol I achieved by modulating the steps in the transcription cycle (initiation, elongation and RNA processing) [33]. Therefore, low processivity of the Pol I may not be an artifact of *in vitro* assays, instead it can be a physiological state with which rRNA synthesis is downregulated. Indeed, upstream binding factor (UBF), which is a homolog of UAF in mammals, was observed to be over-expressed in cancer cells [34, 78]. In our single molecule transcription assays, UAF was absent. It may be speculated that UAF (or UBF) not only regulates initiation step, but alters also rRNA synthesis by decreasing the processivity of Pol I.

5.4 Pol I elongation rate and pausing

It is interesting that in our simplified experimental conditions, which did not involve tension on the DNA template, nor nucleosomes, the pause-free elongation rate

of Pol I was similar to that estimated *in vivo* from EM studies [35]. French *et al.* estimated the Pol I elongation rate by using indirect parameters; yeast generation time, number of ribosomes per cell, number of active rDNA genes, number of polymerases per gene [35]. All the parameters were approximate except the number of polymerases per gene which was a measurement of the EM imaging. Therefore, the *in vivo* rate of 60 nt/s needed to be validated. In contrast, the single molecule assays which was established in this study, directly monitored the movement of the Pol I along the DNA template. One interpretation of this observation is that actively transcribed rDNA repeats are barrier-free *in vivo*. Alternatively, multiple barriers to Pol I transcription elongation may be encountered *in vivo*, but additional trans-acting transcription factors aid the polymerase in negotiating these barriers. Previous studies suggest that several transcription elongation factors influence Pol I activity *in vivo*; however, whether these proteins influence the pause-free velocity of the enzyme remains unclear [73-76]. It is also noteworthy that the elongation rate of Pol I on a supercoiling-free DNA template was found to be comparable to the *in vivo* rate of multiple Pol I molecules on the same rDNA. The tandem order of Pol I molecules on the same gene was speculated to enhance the elongation since the accumulated positive supercoiling ahead of one Pol I can facilitate the generation of negative supercoiling behind the following Pol I [79], which in turn may facilitate binding of new Pol I's to the promoter and new rounds of transcription.

Aside from the epigenetic regulations of active rDNA genes, yeast cells were shown to regulate the rDNA level by altering the elongation rate of Pol I [79]. French *et*

al. demonstrated that the engineered yeast cells which had 40 copies of rDNA instead of 140 copies, maintained the same level of rRNA synthesis and growth with the wild type yeast cells [35]. The recent finding of the crystal structure by Tornero *et al.* revealed that the catalytic core of Pol I is identical to that of Pol II [28]. However, our results depicted that the pause-free elongation rate of Pol I is nearly two folds higher than the *in vivo* rate of Pol II [80] which may be indicative of different mechanisms of transcriptional regulation at individual genes [81]. The transcriptional parameters of Pol I that were obtained in this *in vitro* study and the comparison with the corresponding parameters for Pol II are shown in Table 5.1.

Table 5.1 Transcriptional parameters for Pol I and Pol II. *In vitro* net and pause free rates were established in this study. *In vivo* rate of Pol I was estimated by French *et al.* [35]. Plus (+) and minus (-) signs were used to describe the processivity and homogeneity of the transcriptional complexes. Pol I was found to be not processive *in vitro* and the elongation rate of Pol I was not homogenous. *In vivo* rate and processivity of Pol II were measured by Mason *et al.* [82]. *In vitro* elongation rate of Pol II was measured by Galburt *et al.* [83]. Diversity of transcription by Pol II was observed in [84].

	In vivo rate (bp/s)	In vitro net rate (bp/s)	In vitro pause & backtracking -free rate (bp/s)	Processivity	Homogeneity
Pol I	60	19	51	-	-
Pol II	30	15-20		+	-

Each transcription complex in our TPM assays was prone to pausing (reported as constant tether length over time) and backtracking during the course of each experiment. Sites where a large fraction of complexes have paused may present an intrinsic barrier to the transcription elongation *in vivo* as well. Since it was shown previously that the transcription elongation by Pol I is coupled to rRNA processing, these pause sites could be important for efficiency or regulation of ribosome synthesis. Furthermore, the sequence similarity between the recently revealed prokaryotic pause site (described in section 4.3.3) and the 163 bp location on rDNA may exhibit a conserved pausing signature among the all domains of the life [65]. In addition to that, an pausing event was observed that is called as promoter proximal pause for Pol II on various genes [63, 85]. The most dominant pausing event detected around 200 bp downstream of the promoter for Pol I may indicate a functional similarity between the common pausing event of Pol II.

References

1. Kühnemuth, R. and C.A. Seidel, *Principles of single molecule multiparameter fluorescence spectroscopy*. Single Molecules, 2001. **2**(4): p. 251-254.
2. Schafer, D.A., J. Gelles, M.P. Sheetz, and R. Landick, *TRANSCRIPTION BY SINGLE MOLECULES OF RNA-POLYMERASE OBSERVED BY LIGHT-MICROSCOPY*. Nature, 1991. **352**(6334): p. 444-448.
3. Ritort, F., *Single-molecule experiments in biological physics: methods and applications*. Journal of Physics: Condensed Matter, 2006. **18**(32): p. R531.
4. Nelson, P.C., C. Zurla, D. Brogioli, J.F. Beausang, L. Finzi, and D. Dunlap, *Tethered Particle Motion as a Diagnostic of DNA Tether Length*. The Journal of Physical Chemistry B, 2006. **110**(34): p. 17260-17267.
5. Dietrich, H.R., B. Rieger, F.G. Wiertz, F.H. De Groote, H.A. Heering, I.T. Young, and Y. Garini, *Tethered particle motion mediated by scattering from gold nanoparticles and darkfield microscopy*. Journal of Nanophotonics, 2009. **3**(1): p. 031795-031795-17.
6. Nir, G., M. Lindner, and Y. Garini, *Protein-DNA Interactions Studies with Single Tethered Molecule Techniques*, in *Protein Interactions*, D.J. Cai, Editor. 2012, InTech.
7. Vanzi, F., C. Broggio, L. Sacconi, and F.S. Pavone, *Lac repressor hinge flexibility and DNA looping: single molecule kinetics by tethered particle motion*. Nucleic Acids Research, 2006. **34**(12): p. 3409-3420.
8. Dunlap, D., C. Zurla, C. Manzo, and L. Finzi, *Probing DNA topology using tethered particle motion*. Methods Mol Biol, 2011. **783**: p. 295-313.
9. Ober, R.J., S. Ram, and E.S. Ward, *Localization Accuracy in Single-Molecule Microscopy*. Biophysical Journal, 2004. **86**(2): p. 1185-1200.
10. Finzi, L. and D. Dunlap, *Tethered Particle Microscopy*, in *Encyclopedia of Biophysics*, G.K. Roberts, Editor. 2013, Springer Berlin Heidelberg. p. 2579-2582.
11. Segall, D.E., P.C. Nelson, and R. Phillips, *Volume-exclusion effects in tethered-particle experiments: bead size matters*. Physical review letters, 2006. **96**(8): p. 088306.
12. Koonin, E., A. Gorbalenya, and K. Chumakov, *Tentative identification of RNA-dependent RNA polymerases of dsRNA viruses and their relationship to positive strand RNA viral polymerases*. FEBS letters, 1989. **252**(1): p. 42-46.
13. Hurwitz, J., *The Discovery of RNA Polymerase*. Journal of Biological Chemistry, 2005. **280**(52): p. 42477-42485.
14. Clancy, S., *RNA transcription by RNA polymerase: pro-karyotes vs eukaryotes*. Nature Education, 2008. **1**(1).
15. Liao, S., D. Sagher, A.H. Lin, and S. Fang, *Magnesium and manganese specific forms of soluble liver RNA polymerase*. 1969.
16. ROEDER, R.G. and W.J. RUTTER, *Multiple Forms of DNA-dependent RNA Polymerase in Eukaryotic Organisms*. Nature, 1969. **224**(5216): p. 234-237.
17. Keding, C., M. Gniazdowski, J. Mandel Jr, F. Gissinger, and P. Chambon, *α -Amanitin: a specific inhibitor of one of two DNA-dependent RNA polymerase activities from calf thymus*. Biochemical and biophysical research communications, 1970. **38**(1): p. 165-171.
18. Reeder, R.H. and R.G. Roeder, *Ribosomal RNA synthesis in isolated nuclei*. Journal of molecular biology, 1972. **67**(3): p. 433-441.
19. Weinmann, R. and R.G. Roeder, *Role of DNA-dependent RNA polymerase III in the transcription of the tRNA and 5S RNA genes*. Proceedings of the National Academy of Sciences, 1974. **71**(5): p. 1790-1794.

20. Larson, M.H., R. Landick, and S.M. Block, *Single-Molecule Studies of RNA Polymerase: One Singular Sensation, Every Little Step It Takes*. Molecular Cell, 2011. **41**(3): p. 249-262.
21. Ishibashi, T., M. Dangkulwanich, Y. Coello, T.A. Lionberger, L. Lubkowska, A.S. Ponticelli, M. Kashlev, and C. Bustamante, *Transcription factors IIS and IIF enhance transcription efficiency by differentially modifying RNA polymerase pausing dynamics*. Proceedings of the National Academy of Sciences, 2014. **111**(9): p. 3419-3424.
22. Geiger, S.R., K. Lorenzen, A. Schrieck, P. Hanecker, D. Kostrewa, A.J. Heck, and P. Cramer, *RNA polymerase I contains a TFIIIF-related DNA-binding subcomplex*. Mol Cell, 2010. **39**(4): p. 583-94.
23. Gorski, J.J., S. Pathak, K. Panov, T. Kasciukovic, T. Panova, J. Russell, and J.C. Zomerdijk, *A novel TBP-associated factor of SL1 functions in RNA polymerase I transcription*. The EMBO journal, 2007. **26**(6): p. 1560-1568.
24. Yamamoto, R.T., Y. Nogi, J. Dodd, and M. Nomura, *RRN3 gene of Saccharomyces cerevisiae encodes an essential RNA polymerase I transcription factor which interacts with the polymerase independently of DNA template*. The EMBO journal, 1996. **15**(15): p. 3964.
25. Knutson, B.A., J. Luo, J. Ranish, and S. Hahn, *Architecture of the Saccharomyces cerevisiae RNA polymerase I Core Factor complex*. Nat Struct Mol Biol, 2014. **21**(9): p. 810-816.
26. Németh, A., J. Perez-Fernandez, P. Merkl, S. Hamperl, J. Gerber, J. Griesenbeck, and H. Tschochner, *RNA polymerase I termination: Where is the end?* Biochimica et Biophysica Acta (BBA) - Gene Regulatory Mechanisms, 2013. **1829**(3-4): p. 306-317.
27. Kuhn, C.D., S.R. Geiger, S. Baumli, M. Gartmann, J. Gerber, S. Jennebach, T. Mielke, H. Tschochner, R. Beckmann, and P. Cramer, *Functional architecture of RNA polymerase I*. Cell, 2007. **131**(7): p. 1260-1272.
28. Fernández-Tornero, C., M. Moreno-Morcillo, U.J. Rashid, N.M. Taylor, F.M. Ruiz, T. Gruene, P. Legrand, U. Steuerwald, and C.W. Müller, *Crystal structure of the 14-subunit RNA polymerase I*. Nature, 2013. **502**(7473): p. 644-649.
29. Warner, J.R., *The economics of ribosome biosynthesis in yeast*. Trends in biochemical sciences, 1999. **24**(11): p. 437-440.
30. Schneider, D.A., A. Michel, M.L. Sikes, L. Vu, J.A. Dodd, S. Salgia, Y.N. Osheim, A.L. Beyer, and M. Nomura, *Transcription Elongation by RNA Polymerase I Is Linked to Efficient rRNA Processing and Ribosome Assembly*. Molecular Cell, 2007. **26**(2): p. 217-229.
31. Viktorovskaya, O.V., K.L. Engel, S.L. French, P. Cui, P.J. Vandeventer, E.M. Pavlovic, A.L. Beyer, C.D. Kaplan, and D.A. Schneider, *Divergent contributions of conserved active site residues to transcription by eukaryotic RNA polymerases I and II*. Cell reports, 2013. **4**(5): p. 974-984.
32. Engel, C., S. Sainsbury, A.C. Cheung, D. Kostrewa, and P. Cramer, *RNA polymerase I structure and transcription regulation*. Nature, 2013. **502**(7473): p. 650-655.
33. Drygin, D., W.G. Rice, and I. Grummt, *The RNA polymerase I transcription machinery: an emerging target for the treatment of cancer*. Annu Rev Pharmacol Toxicol, 2010. **50**: p. 131-56.
34. Bywater, Megan J., G. Poortinga, E. Sanij, N. Hein, A. Peck, C. Cullinane, M. Wall, L. Cluse, D. Drygin, K. Anderes, N. Huser, C. Proffitt, J. Bliesath, M. Haddach, Michael K. Schwaebe, David M. Ryckman, William G. Rice, C. Schmitt, Scott W. Lowe, Ricky W. Johnstone, Richard B. Pearson, Grant A. McArthur, and Ross D. Hannan, *Inhibition of RNA Polymerase I as a Therapeutic Strategy to Promote Cancer-Specific Activation of p53*. Cancer Cell, 2012. **22**(1): p. 51-65.
35. French, S.L., Y.N. Osheim, F. Cioci, M. Nomura, and A.L. Beyer, *In exponentially growing Saccharomyces cerevisiae cells, rRNA synthesis is determined by the summed RNA*

- polymerase I loading rate rather than by the number of active genes.* Molecular and cellular biology, 2003. **23**(5): p. 1558-1568.
36. Han, L., B.H. Lui, S. Blumberg, J.F. Beausang, P.C. Nelson, and R. Phillips, *Calibration of tethered particle motion experiments*, in *Mathematics of DNA structure, function and interactions*. 2009, Springer. p. 123-138.
 37. Wang, M.D., H. Yin, R. Landick, J. Gelles, and S.M. Block, *Stretching DNA with optical tweezers*. Biophysical journal, 1997. **72**(3): p. 1335-1346.
 38. Yin, H., R. Landick, and J. Gelles, *Tethered particle motion method for studying transcript elongation by a single RNA polymerase molecule*. Biophysical journal, 1994. **67**(6): p. 2468-2478.
 39. Pyun, J., *Single-molecule studies of active and static transcription complexes*. 2005, Brandeis University: United States -- Massachusetts. p. 135 p.
 40. Sandip Kumar, C.M., Chiara Zurla, Suleyman Ucuncuoglu, Laura Finzi and David Dunlap, *Enhanced Tethered-Particle Motion Analysis Reveals Viscous Effects*. Biophysical Journal, 2014. **106**(January 2014): p. 1-11.
 41. Zurla, C., A. Franzini, G. Galli, D. Dunlap, D. Lewis, S. Adhya, and L. Finzi, *Novel tethered particle motion analysis of CI protein-mediated DNA looping in the regulation of bacteriophage lambda*. Journal of Physics: Condensed Matter, 2006. **18**(14): p. S225.
 42. Lazinski, D.W. and J.M. Taylor, *Intracellular cleavage and ligation of hepatitis delta virus genomic RNA: regulation of ribozyme activity by cis-acting sequences and host factors*. Journal of virology, 1995. **69**(2): p. 1190-1200.
 43. Wang, H., L. Finzi, D.E. Lewis, and D. Dunlap, *AFM studies of λ repressor oligomers securing DNA loops*. Current pharmaceutical biotechnology, 2009. **10**(5): p. 494.
 44. Destainville, N. and L. Salomé, *Quantification and correction of systematic errors due to detector time-averaging in single-molecule tracking experiments*. Biophysical journal, 2006. **90**(2): p. L17-L19.
 45. Blumberg, S., A. Gajraj, M.W. Pennington, and J.-C. Meiners, *Three-dimensional characterization of tethered microspheres by total internal reflection fluorescence microscopy*. Biophysical journal, 2005. **89**(2): p. 1272-1281.
 46. Lindner, M., G. Nir, S. Medalion, H.R. Dietrich, Y. Rabin, and Y. Garini, *Force-free measurements of the conformations of DNA molecules tethered to a wall*. Physical Review E, 2011. **83**(1): p. 011916.
 47. Han, L., B.H. Lui, S. Blumberg, J.F. Beausang, P.C. Nelson, and R. Phillips, *Calibration of Tethered Particle Motion Experiments*, in *Mathematics of DNA Structure, Function and Interactions*, C.J. Benham, S. Harvey, W.K. Olson, D.W.L. Sumners, and D. Swigon, Editors. 2009, Springer: New York. p. 123-138.
 48. Milstein, J.N., Y.F. Chen, and J.C. Meiners, *Bead size effects on protein-mediated DNA looping in tethered-particle motion experiments*. Biopolymers, 2011. **95**(2): p. 144-50.
 49. Pouget, N., C. Dennis, C. Turlan, M. Grigoriev, M. Chandler, and L. Salome, *Single-particle tracking for DNA tether length monitoring*. Nucleic Acids Res, 2004. **32**(9): p. e73.
 50. Laurens, N., S.R.W. Bellamy, A.F. Harms, Y.S. Kovacheva, S.E. Halford, and G.J.L. Wuite, *Dissecting protein-induced DNA looping dynamics in real time*. Nucleic Acids Research, 2009. **37**(16): p. 5454-5464.
 51. Zurla, C., C. Manzo, D. Dunlap, D.E. Lewis, S. Adhya, and L. Finzi, *Direct demonstration and quantification of long-range DNA looping by the lambda bacteriophage repressor*. Nucleic Acids Res, 2009. **37**(9): p. 2789-95.
 52. Plénat, T., C. Tardin, P. Rousseau, and L. Salomé, *High-throughput single-molecule analysis of DNA-protein interactions by tethered particle motion*. Nucleic acids research, 2012: p. gks250.

53. Aprikian, P., B. Moorefield, and R.H. Reeder, *New model for the yeast RNA polymerase I transcription cycle*. Molecular and cellular biology, 2001. **21**(15): p. 4847-4855.
54. Schneider, D.A., *Quantitative analysis of transcription elongation by RNA polymerase I in vitro*. Methods Mol Biol, 2012. **809**: p. 579-91.
55. Parthasarathy, R., *Rapid, accurate particle tracking by calculation of radial symmetry centers*. Nature Methods, 2012. **9**(7): p. 724-726.
56. Qian, H., M.P. Sheetz, and E.L. Elson, *Single particle tracking. Analysis of diffusion and flow in two-dimensional systems*. Biophysical journal, 1991. **60**(4): p. 910-921.
57. Yin, H., I. Artsimovitch, R. Landick, and J. Gelles, *Nonequilibrium mechanism of transcription termination from observations of single RNA polymerase molecules*. Proceedings of the National Academy of Sciences, 1999. **96**(23): p. 13124.
58. Gellert, M., K. Mizuuchi, M.H. O'Dea, and H.A. Nash, *DNA gyrase: an enzyme that introduces superhelical turns into DNA*. Proceedings of the National Academy of Sciences, 1976. **73**(11): p. 3872-3876.
59. Klein, J. and I. Grummt, *Cell cycle-dependent regulation of RNA polymerase I transcription: the nucleolar transcription factor UBF is inactive in mitosis and early G1*. Proceedings of the National Academy of Sciences, 1999. **96**(11): p. 6096-6101.
60. Grummt, I., *Regulation of mammalian ribosomal gene transcription by RNA polymerase I*. Progress in nucleic acid research and molecular biology, 1998. **62**: p. 109-154.
61. Cramer, P., K.J. Armache, S. Baumli, S. Benkert, F. Brueckner, C. Buchen, G. Damsma, S. Dengl, S. Geiger, and A. Jasiak, *Structure of eukaryotic RNA polymerases*. Annu. Rev. Biophys., 2008. **37**: p. 337-352.
62. Schneider, D., S. French, Y. Osheim, A. Bailey, L. Vu, J. Dodd, J. Yates, A. Beyer, and M. Nomura, *RNA polymerase II elongation factors Spt4p and Spt5p play roles in transcription elongation by RNA polymerase I and rRNA processing*. Proceedings of the National Academy of Sciences, 2006. **103**(34): p. 12707-12712.
63. Adelman, K. and J.T. Lis, *Promoter-proximal pausing of RNA polymerase II: emerging roles in metazoans*. Nature Reviews Genetics, 2012. **13**(10): p. 720-731.
64. Keener, J., C.A. Josaitis, J.A. Dodd, and M. Nomura, *Reconstitution of yeast RNA polymerase I transcription in vitro from purified components*. Journal of Biological Chemistry, 1998. **273**(50): p. 33795-33802.
65. Larson, M.H., R.A. Mooney, J.M. Peters, T. Windgassen, D. Nayak, C.A. Gross, S.M. Block, W.J. Greenleaf, R. Landick, and J.S. Weissman, *A pause sequence enriched at translation start sites drives transcription dynamics in vivo*. Science, 2014. **344**(6187): p. 1042-1047.
66. Neuman, K.C., E.A. Abbondanzieri, R. Landick, J. Gelles, and S.M. Block, *Ubiquitous transcriptional pausing is independent of RNA polymerase backtracking*. Cell, 2003. **115**(4): p. 437-447.
67. Tolic-Norrelykke, S.F., A.M. Engh, R. Landick, and J. Gelles, *Diversity in the rates of transcript elongation by single RNA polymerase molecules*. J Biol Chem, 2004. **279**(5): p. 3292-9.
68. Kool, E.T., *Hydrogen bonding, base stacking, and steric effects in DNA replication*. Annual review of biophysics and biomolecular structure, 2001. **30**(1): p. 1-22.
69. Bommarito, S., N. Peyret, and J. SantaLucia Jr, *Thermodynamic parameters for DNA sequences with dangling ends*. Nucleic Acids Research, 2000. **28**(9): p. 1929-1934.
70. Xie, S., *Single-molecule approach to enzymology*. Single Molecules, 2001. **2**(4): p. 229-236.
71. Robison, A.D. and I.J. Finkelstein, *High-throughput single-molecule studies of protein-DNA interactions*. FEBS Letters, 2014. **588**(19): p. 3539-3546.
72. Ribbeck, N. and O.A. Saleh, *Multiplexed single-molecule measurements with magnetic tweezers*. Review of Scientific Instruments, 2008. **79**(9): p. 094301.

73. Zhang, Y., S.J. Anderson, S.L. French, M.L. Sikes, O.V. Viktorovskaya, J. Huband, K. Holcomb, J.L. Hartman IV, A.L. Beyer, and D.A. Schneider, *The SWI/SNF Chromatin Remodeling Complex Influences Transcription by RNA Polymerase I in Saccharomyces cerevisiae*. PLoS one, 2013. **8**(2): p. e56793.
74. Zhang, Y., M.L. Sikes, A.L. Beyer, and D.A. Schneider, *The Paf1 complex is required for efficient transcription elongation by RNA polymerase I*. Proceedings of the National Academy of Sciences, 2009. **106**(7): p. 2153-2158.
75. Zhang, Y., A.D. Smith, M.B. Renfrow, and D.A. Schneider, *The RNA polymerase-associated factor 1 complex (Paf1C) directly increases the elongation rate of RNA polymerase I and is required for efficient regulation of rRNA synthesis*. Journal of biological chemistry, 2010. **285**(19): p. 14152-14159.
76. Anderson, S.J., M.L. Sikes, Y. Zhang, S.L. French, S. Salgia, A.L. Beyer, M. Nomura, and D.A. Schneider, *The transcription elongation factor Spt5 influences transcription by RNA polymerase I positively and negatively*. Journal of Biological Chemistry, 2011. **286**(21): p. 18816-18824.
77. El Hage, A., S.L. French, A.L. Beyer, and D. Tollervey, *Loss of Topoisomerase I leads to R-loop-mediated transcriptional blocks during ribosomal RNA synthesis*. Genes & development, 2010. **24**(14): p. 1546-1558.
78. Hannan, K.M., L.I. Rothblum, and L.S. Jefferson, *Regulation of ribosomal DNA transcription by insulin*. American Journal of Physiology-Cell Physiology, 1998. **275**(1): p. C130-C138.
79. Russell, J. and J.C. Zomerdijk, *RNA-polymerase-I-directed rDNA transcription, life and works*. Trends in biochemical sciences, 2005. **30**(2): p. 87-96.
80. Liu, X., D.A. Bushnell, and R.D. Kornberg, *RNA polymerase II transcription: structure and mechanism*. Biochimica et Biophysica Acta (BBA)-Gene Regulatory Mechanisms, 2013. **1829**(1): p. 2-8.
81. Sandmeier, J.J., S. French, Y. Osheim, W.L. Cheung, C.M. Gallo, A.L. Beyer, and J.S. Smith, *RPD3 is required for the inactivation of yeast ribosomal DNA genes in stationary phase*. The EMBO journal, 2002. **21**(18): p. 4959-4968.
82. Mason, P.B. and K. Struhl, *Distinction and Relationship between Elongation Rate and Processivity of RNA Polymerase II In Vivo*. Molecular Cell, 2005. **17**(6): p. 831-840.
83. Galburt, E.A., S.W. Grill, A. Wiedmann, L. Lubkowska, J. Choy, E. Nogales, M. Kashlev, and C. Bustamante, *Backtracking determines the force sensitivity of RNAP[thinsp]II in a factor-dependent manner*. Nature, 2007. **446**(7137): p. 820-823.
84. Ardehali, M.B., J. Yao, K. Adelman, N.J. Fuda, S.J. Petesch, W.W. Webb, and J.T. Lis, *Spt6 enhances the elongation rate of RNA polymerase II in vivo*. The EMBO Journal, 2009. **28**(8): p. 1067-1077.
85. Core, L.J. and J.T. Lis, *Transcription regulation through promoter-proximal pausing of RNA polymerase II*. Science, 2008. **319**(5871): p. 1791-1792.